

EFFECTS OF FERROMAGNETIC LAYERS UPON TUNNELING
IN SUPERCONDUCTING LEAD JUNCTIONS

By

JOE FRANCIS GUESS

Bachelor of Science
Bethany Nazarene College
Bethany, Oklahoma
1960

Master of Science
Oklahoma State University
Stillwater, Oklahoma
1963

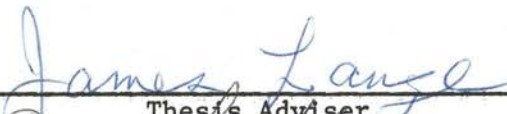
Submitted to the Faculty of the Graduate College
of the Oklahoma State University
in partial fulfillment of the requirements
of the Degree of
DOCTOR OF PHILOSOPHY
May, 1972

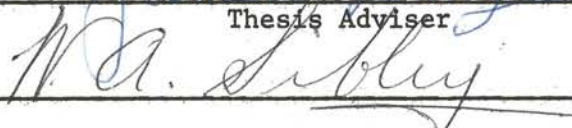
Thesis
19720
G936e
cap. 2

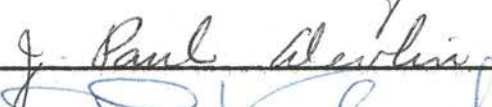
AUG 10 1973


EFFECTS OF FERROMAGNETIC LAYERS UPON TUNNELING
IN SUPERCONDUCTING LEAD JUNCTIONS

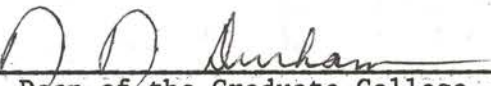
Thesis Approved:



Thesis Adviser








Dean of the Graduate College

ACKNOWLEDGEMENTS

The author wishes to thank some of the persons who have been helpful in the completion of this research. Dr. James Lange gave meaningful direction and was a very pleasant person with whom to work. Wayne Adkins was invaluable for the research in doing the glass work on the vacuum system and keeping things going when the inevitable breaks in dewars and pumping lines occurred. Heinz Hall, Frank Hargrove, Floyd Vulgamore, and Richard Gruhlkey have been indispensable fabricating machined items from sample holder to vacuum apparatus and giving helpful design advice. The financial support of the National Science Foundation has allowed a higher degree of concentration on the work.

I am thankful to Mary, Mary Frances and Kathy for their understanding, love and appreciation, and for just making life enjoyable.

TABLE OF CONTENTS

Chapter	Page
I. INTRODUCTION.	1
II. EXPERIMENTAL TECHNIQUES	10
Sample Preparation	10
Tunneling Measurements	24
III. TUNNELING IN Pb-I-Pb JUNCTIONS.	34
Single Particle Tunneling Effects.	34
Pair Tunneling Effects	41
IV. FERROMAGNETIC MATERIAL IN TUNNELING JUNCTIONS	54
Iron-Lead Tunneling and the Proximity Effect	56
Various Effects in Superconducting Junctions Con- taining Ferromagnetic Material	62
V. SUMMARY AND SUGGESTED FURTHER WORK.	70
BIBLIOGRAPHY.	72

LIST OF FIGURES

Figure	Page
1. Typical Tunneling Junction Sample.	10
2. Diagram of Vacuum and Gas Handling System.	13
3. Evaporation Chamber.	16
4. Constant Density Contours of the Fringe Pattern of a 100Å ⁰ Step in Film Thickness	19
5. Spectra From Glow Discharge With and Without Contaminant Lines Visible.	22
6. Circuit for Junction Testing	25
7. Circuit of Temperature Controller.	27
8. Circuit for Oscilloscope Display of Current-Voltage Char- acteristics.	29
9. Photograph of Sample Holder.	30
10. Dewar and Magnet Systems	32
11. Current and Derivative Characteristics of a Pb-I-Pb Junc- tion at 4.2°K.	35
12. Semiconductor Model of Tunneling Experiment.	36
13. Temperature Variation of Low emf Tunneling Current	38
14. Expanded Derivative in the Region of Phonon Density Ef- fects.	40
15. Magnetic Field Dependence of Maximum Supercurrent in a Low Resistance Junction.	46
16. Fiske Modes Detected in the Characteristics of the Junc- tion of Figure 15.	48
17. Relationship Between Fiske Mode Velocity and Junction Re- sistance for a Number of Junctions	50
18. Subharmonic Structure in Two Junctions	52

LIST OF FIGURES (Continued)

Figure	Page
19. Diagrams of Film Configurations.	55
20. Derivative Characteristics of a $\text{Fe-Fe}_x\text{O}_y$ Junction	57
21. The Effects of Magnetic Films Outside the Junction on Tunneling Characteristics.	59
22. Normalized Density of States Induced at the Fermi Level by the Proximity Effect as a Function of Lead Thickness . . .	61
23. Derivative Curves for Two Pb-I-Fe-I-Pb Samples	64
24. Characteristics of Junctions Containing Fe in Contact with Pb but Within the Barrier.	66
25. Field Dependence of the Resistance Peaks Shown in Figure 24	67
26. High Resistance Spikes in dV/dI of #227J3 a) Shown Super- imposed on the Phonon Structure and b) Magnetic Field at Which Peaks Appear vs. emf of Peak.	69

LIST OF SYMBOLS

a_1, a_2	inner and outer radii of solenoid windings
B	magnetic field intensity
c	speed of light in vacuum
d	tunneling barrier thickness
E	energy of particle state
e	electronic charge
h	Plank's constant
\hbar	$h/2\pi$
I	current
I_s	supercurrent
J	current density
J_s	supercurrent density
l	length of solenoid windings
N	density of electronic states
n	integer as defined in text
R	normalized density of states at center of energy gap
r	coordinate vector
t	time
V	junction emf
v	electromagnetic wave velocity within barrier
w	lateral junction dimension
ϵ	dielectric constant

LIST OF SYMBOLS (Continued)

Δ	superconducting energy gap
σ_{NT}	junction normal state conductance per unit area
ξ	coherence length
λ	penetration depth
Φ	magnetic flux
Φ_0	one flux quantum
ϕ	phase of Ginzburg-Landau order parameter
Ψ	Ginzburg-Landau order parameter
μ	chemical potential
μ_0	permeability of free space
ω	angular frequency

CHAPTER I

INTRODUCTION

Since Giaever (1) first used tunneling to directly measure the energy gap and density of states of superconductors, tunneling between superconductors or between a superconductor and a normal metal has been a sensitive probe to the superconducting state. Superconducting tunneling junctions have also been used in very sensitive gaussmeters and voltmeters and in precise determination of fundamental constants (2-5). Because of the low switching time between the pair tunneling and single particle tunneling states, tunneling junctions have been proposed as computer elements in logic operations (6).

The tunneling technique is used in this study to measure changes in the superconducting state due to a ferromagnetic film in contact with the superconductor, and it is found that there is an energy spread of the superconducting state which decreases with increasing distance from the magnetic film.

Tunneling junctions are fabricated so that the superconductor and normal metal or other superconductor are separated by a very thin ($10\text{-}50\text{\AA}$) insulating barrier. Current across the insulator is classically forbidden, but the tunneling current that is measured is understood on the basis of wave mechanics and the fundamental impossibility of precisely locating a particle in space. The significant probability that the current carrying particle will appear on the other side of the in-

insulating barrier gives rise to a measurable current.

The power of the tunneling technique arises from its energy discrimination. The most probable mechanism for a particle to tunnel across the barrier is one which does not require radiation or absorption of energy and energy is therefore conserved. If an arbitrary emf V is applied across the barrier, the energies of particles of charge q on one side of the barrier are changed with respect to some energy level on the other side by an amount qV . Thus tunneling current into any energy level can be studied by choosing the proper emf.

In addition to the tunneling mechanism other factors influencing tunneling probability are the numbers of available particles and of available states into which the particle can tunnel. Since calculations of the probability of the energy conserving mechanism on the basis of simple models are insensitive to energy, the structure in tunneling current-voltage characteristics is primarily due to variation with energy of the number of states per unit energy.

The junctions may be point contacts on bulk material or thin films, but the most common form is an insulating barrier between two thin films (7-10). The thin insulating barrier is usually produced on thin films by oxidation of the first layer: exposing the film to the atmosphere, heating in an oxygen atmosphere, or exposing to a glow discharge in oxygen (1, 5, 11-13). The surface oxidation process has been studied in detail for Pb (14-16). Polymer films have also been used as insulating barriers (17-18).

The theory of superconductivity proposed by Bardeen, Cooper and Schrieffer (19) was the first to successfully predict the wealth of macroscopic effects which had been observed in terms of a microscopic

theory. They simplified the basic mechanism of an attractive interaction between electrons via lattice vibrations to an instantaneous, small attractive potential, and were then able to predict that when a material goes from the normal state to the superconducting state, the highest energy electrons (near the Fermi level) condense in pairs into a new state an energy Δ per electron below the Fermi energy, and a gap of Δ either side of the Fermi energy appears in the excitation spectrum.

The most obvious feature of the current vs. voltage characteristic of a tunneling junction between superconductors is the result of this superconducting energy gap. For applied voltages such that $eV < 2\Delta$ the tunneling currents are very low, and at 2Δ gap the current suddenly increases as the superconducting pairs on one side of the junction can break up and tunnel into the empty states on the other side. The energy gaps of various materials have been measured and the temperature dependence has been compared with the BCS theory (20-26). The tunneling technique has been used to measure the energy gap in crystalline and amorphous materials and in alloys (27-29).

The sensitivity of the tunneling technique became apparent in the investigation of the electron-phonon interaction. In 1961 Giaever (21) reported small but significant (~ 10%) deviations in the density of states of Pb from that predicted by the BCS theory. Since it had been suggested by Anderson (30) that there might be effects of phonon scattering in the anomalous heavy metal superconductors, there was simultaneous experimental and theoretical activity to describe the observations in terms of assumed densities of phonon states and the Eliashberg (31) theory (31-40). This generalized theory of superconductivity predicts a complex energy gap and a density of states which are functions

of energy by taking into account an electron-phonon interaction which is not small and is retarded in time. McMillan and Rowell (41) were successful in devising a method to invert the Eliashberg equations and generate the density of phonon states from the experimental data. These results have been compared to those derived from neutron diffraction data in Pb (42). Some discrepancies have been identified as defects in the model used to reduce the neutron diffraction data and resolved with more complete neutron diffraction data (43-46). Phonon effects have been detected and analyzed in weak-coupling superconductors in addition to the further investigation of the heavy metals (24, 47-51).

Another effect which is observed in the I-V characteristic of a tunneling junction between two superconductors was predicted theoretically by Josephson (52), and first clearly observed and characterized by Anderson and Rowell (53, 54). In the dc Josephson effect, a tunneling supercurrent can be observed with no voltage appearing across the junction. This current has a maximum value which is sensitive to magnetic fields on the order of a gauss and shows a Fraunhofer diffraction like dependence on them (55, 56). For current levels higher than this maximum the junction switches to conduction by the single particle mechanism with the resultant appearance of an emf across the junction. The usual maximum supercurrents reported by many observers (33, 53, 54, 57-61) are significantly reduced by the self-field of the current, strong coupling effects in the superconductors, and thermal noise (16, 55, 59-64). It has been shown that a noise voltage across the junction appears because of thermal fluctuations of the supercurrent (65, 66). Paramagnetic impurities can also reduce the maximum supercurrent (67). Dynes and Fulton (68) have used the variations from the Fraunhofer diffraction pattern to

experimentally determine profiles of the supercurrent density across tunneling junctions.

The exposure of a junction in which pair tunneling is observed to microwave radiation induces current steps in the tunneling I-V characteristic around zero bias at equally spaced voltages $V_n = n\hbar\omega/2e$ where n is an integer. These pair tunneling steps were first observed by Shapiro (69) after the experiment was suggested by Josephson (64). Current steps have also been observed in the vicinity of the energy gap with $\Delta V = \hbar\omega/e$ and are due to photon-assisted single particle tunneling (70). Both of these effects have been described in detail including the dependence upon rf voltage (69-76). Because of the direct relationship between the junction voltage and the rf frequency in the ac Josephson effect, Langenberg et. al. (5, 77) have used the interaction in a precise measurement of the fundamental constant h/e .

Tunneling junctions can also radiate by a pair tunneling process where the emitted photon has energy $2eV$, where V is the emf between sides of the junction. Because of the lower probability of tunneling with photon emission, the currents are much lower than in the direct process, but Fiske (78, 79) was able to observe current steps in the microvolt region corresponding to electromagnetic resonant frequencies of the junction dimensions. The emitted radiation corresponding to one of these modes was detected by Yanson (80) at a power level on the order of 10^{-14} W. Noise and bandwidth effects in this radiation have been considered (81, 82). Kamper and Zimmerman (83) have recently proposed using the bandwidth of this radiation as a thermometer in the millidegree range.

It now appears that another striking feature of superconducting

tunneling junctions is due to self-detection of the emitted radiation (84). A current step in the I-V characteristic at $eV = \Delta$ was reported and at first explained in terms of a multiparticle tunneling mechanism (85-88). However, other structure was soon encountered by Yanson and collaborators (89) in the I-V characteristic at further voltages $eV_n = 2\Delta/n$ where V_n is the junction emf associated with the nth subharmonic, and was observed by many investigators for n as high as 12 (8, 90, 91). The multiparticle tunneling model could not satisfactorily describe the occurrence of the higher submultiples nor the high probability of the effect. Harmonic generation of applied rf power has been observed, substantiating the non-linearity of the ac effect and the self-detection model (92).

In thick films a structure around the energy gap which is periodic in voltage was discovered in tunneling measurements by Tomasch (93). The geometrically dependent periodicity is explained as interference of electron-like and hole-like excitations of equal energy and nearly equal k vectors (94, 95). At much higher energies Jaklevic et. al. (96) report the observation of detail in the 0.4 to 1.2 volt range of tunneling characteristics due to resonance of electron k vectors with the film thickness. This effect was observed in both normal and superconducting films.

When in addition to the superconducting films and the presumably inert insulating barrier, other materials are in the vicinity of the gap, numerous interactions take place depending upon the concentration, location and type of impurity. Jaklevic and Lambe (97, 98) have studied extensively molecular impurities within the barrier layer by the interaction of the vibrational modes of the molecule and the tunneling electron.

The additional tunneling mechanism which becomes active at $eV = 2\Delta + \hbar\omega_0$, where $\hbar\omega_0$ is the energy of the vibrational mode, is reflected in an increased conductance in the tunneling characteristic. The work has been extended to vibrational modes of oxides (99). Caswell (100) found that specific gaseous impurities present during depositions of Sn films altered their magnetic transitions, but in other studies (61) even higher gaseous impurities in Pb have not altered the tunneling characteristics. Inclusion of Cu, Ag and Au impurities in Sn films contributes to crystalline disorder, increases the transition temperature and alters the phonon induced density of excited states structure, as would be expected since the crystalline disorder modifies the phonon spectrum (28).

A possibly related effect appears in normal metal tunneling junctions [studied extensively by Giaever et. al. (101)] where the dynamic resistances have been observed to have a temperature dependent peak about zero junction voltage (102, 103). This zero bias anomaly has been explained in terms of magnetic impurities within the barrier layer, and recent experiments with paramagnetic and ferromagnetic materials have shown the effect (104-107). However, another mechanism involving the capacitance of small particles of the impurities has been proposed and given experimental support by Zeller and Giaever (108).

Magnetic impurities within the superconductor have been found to strongly decrease the transition temperature of superconductors, and a region of impurity concentration was predicted for which the excitation spectrum of the superconducting state is gapless (109-111). Due to the long range order of the superconducting state, the case of surface impurities on a thin superconducting film is closely related to the case

of included impurities. For example, Wolf and Reif (112), who studied both surface and included impurities, found that 15\AA of Fe on a 500\AA In film completely eliminated the gap in the energy spectrum. A theory of the superconductor-magnetic alloys has been obtained by extension from McMillan's (113) theory of superconductor-normal metal proximity effect (114). The latter case with the characteristic induced gap in the normal metal has been studied extensively in experiment and theory (114-122). There is disagreement in the measurements on superconductors in contact with ferrimagnetic, ferromagnetic or anti-ferromagnetic materials as to the magnitudes of the depression of the critical temperature and the smearing of the energy gap (112, 123-126). The details of sample preparation including the presence of thin barriers, or diffusion of the metals are probably responsible (119, 127).

Hauser and collaborators (121, 124, 128, 129) are responsible for intensive experimental work on the subject of magnetic-superconductor thin film sandwiches. In his 1967 paper using the tunneling technique to measure the density of states at the center of the gap as a function of temperature, Hauser obtained a relationship which, when normalized to the transition temperature of the composite sandwich, is independent of the metal applied to the sandwich whether a ferromagnetic or normal metal, in agreement with a theory by Fulde and Maki (130).

The experimental and theoretical analysis of metal-superconductor sandwiches typically considers the density of states of the superconductor to be modified by the same amount throughout its thickness. It is well known that although the superconducting state is non-local, its extent, characterized by the coherence length ξ , is on the order of film thicknesses used in experiments. This variation of the states induced

by the presence of the magnetic film is experimentally verified in this study, and allows a direct measure of ξ .

Expecting a phonon-assisted tunneling analogy to the Dayem-Martin (70) effect of photon-assisted tunneling, early investigators (10, 132, 133) irradiated superconducting tunneling junctions with phonons of microwave frequencies and looked for a step-like structure in the tunneling characteristic. However, there were no clearly defined steps in the measured change in current $\delta I(V)$ with application of acoustic power, although the change in current was claimed to be conclusively identified as phonon-assisted tunneling (133). Other investigators measured a similar variation of δI (approximately proportional to d^2I/dV^2) with a different power dependence at higher powers (134, 135). Cohen (136) extended the calculation of the effect of a periodic perturbation on the superconductor to include the Eliashberg electron-phonon interaction, and accounts for some discrepancies between experiment and theory.

Tunneling junctions have been used as generators and detectors of incoherent phonons in some experiments that bypass the piezoelectric transducer and its frequency limitations (137-139). In Eisenmenger's (137) experiment the phonons generated when electrons recombine to form Cooper pairs propagate down a sapphire rod and impinge on another junction to excite a pair of electrons across the energy gap and increase their tunneling probability. The phonon generation mechanism is discussed by Trewordt (140). The experiments by Schulz and Weis (139) in which heat pulses are detected with superconducting tunnel junctions show that these devices are suitable detectors of phonons above the energy gap.

CHAPTER II

EXPERIMENTAL TECHNIQUES

Sample Preparation

The tunnel junctions used throughout this study were produced using thin film techniques in an oil diffusion pumped evaporation system. A

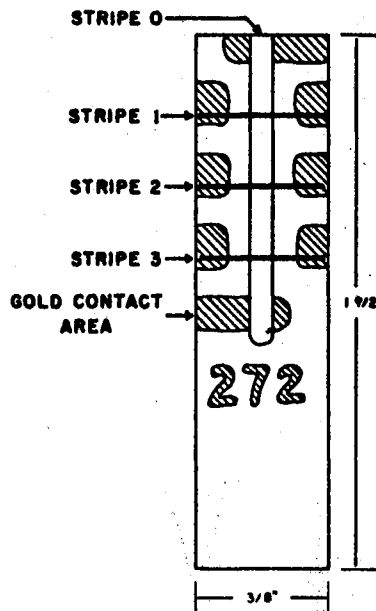


Figure 1. Typical Tunneling Junction Sample

typical sample is shown in Figure 1. The substrate is a section of a microscope slide which has gold contact areas baked on prior to junction fabrication. The evaporated lead stripe 0 is oxidized by heating or exposure to a glow discharge in an oxygen atmosphere. This produces an

insulating barrier at the surface over which the cross stripes are evaporated to form a sandwich: superconductor-insulator-superconductor or S-I-S. Another metallic film, normal or ferromagnetic metal, may be evaporated at any point in the processing introducing that material into the sandwich. Such combinations as M·S·I·S, S·M·I·S, and S·I·S·M have been used.

Substrate Preparation

The substrates are formed by scribing standard 1" x 3" microscope slides with a diamond tip scribe and breaking to the 3/8" x 1 1/4" size. Bright Gold, an Englehard product, is then painted on the substrates with an artist's brush and fired at 550°C for 2 hrs to form the contact areas. The identification number is put on the substrate with Bright Gold also.

The substrates are cleaned by individually scrubbing each one in a hot Alconox solution and placing them in a Teflon holder which is designed to contact only two edges of the glass and allow free draining. All handling is done with tweezers to prevent skin oils from contaminating the glass surface. The holder is kept immersed in water so the substrates are never allowed to dry after the first scrub. The end of the substrate upon which the film will be evaporated is oriented upward so that contaminants will drain away from that area. The procedure then is as follows: the initial scrub, two washes in hot Alconox solution, two hot tap water rinses, three distilled water rinses, an ethyl alcohol rinse and a degreasing with isopropyl alcohol vapor. Two beakers are reserved for the cleaning operation and the cleaning steps are alternated between them. Each is carefully rinsed twice with the

solvent to be used in the next cleaning step before filling with that solvent.

Vacuum and Gas Handling Apparatus

The vacuum system which is diagrammed in Figure 2 has a pumping speed measured with O_2 of one liter/sec at 10^{-3} torr, ultimate pressure near 3×10^{-7} torr without a prior bake out and a pressure during evaporation of Pb films less than 2×10^{-6} . The liquid nitrogen cold finger is chilled continuously except for occasional degass periods.

Gases for oxidation or sputtering can be admitted to the system either in continuous flow or measured amounts. Control of the flow rate is achieved by regulating the pressure of the gas admitted to the flow capillary. This capillary was drawn so that argon pressures of 0 - 50 psi above atmospheric pressure produce system pressures of 10 - 200 microns at maximum pumping rates. Fine control of pressure is achieved by using the gate valve to throttle the pumping rate. Discrete amounts of gases may be admitted by filling the metric capillary to a particular pressure and opening it to the system. The capillary has an approximate volume of 70 mm^3 and one capillary at 32 psi above atmospheric pressure produces a system pressure of 100 microns with the gate-valve closed. Gas can be admitted at high flow rates by flowing through the metric capillary and controlling the flow rate with the needle valve on the oxygen regulator. Gas pressures are routinely measured with the thermocouple gauge.

Evaporations

The superconducting films of lead, the material which is common to

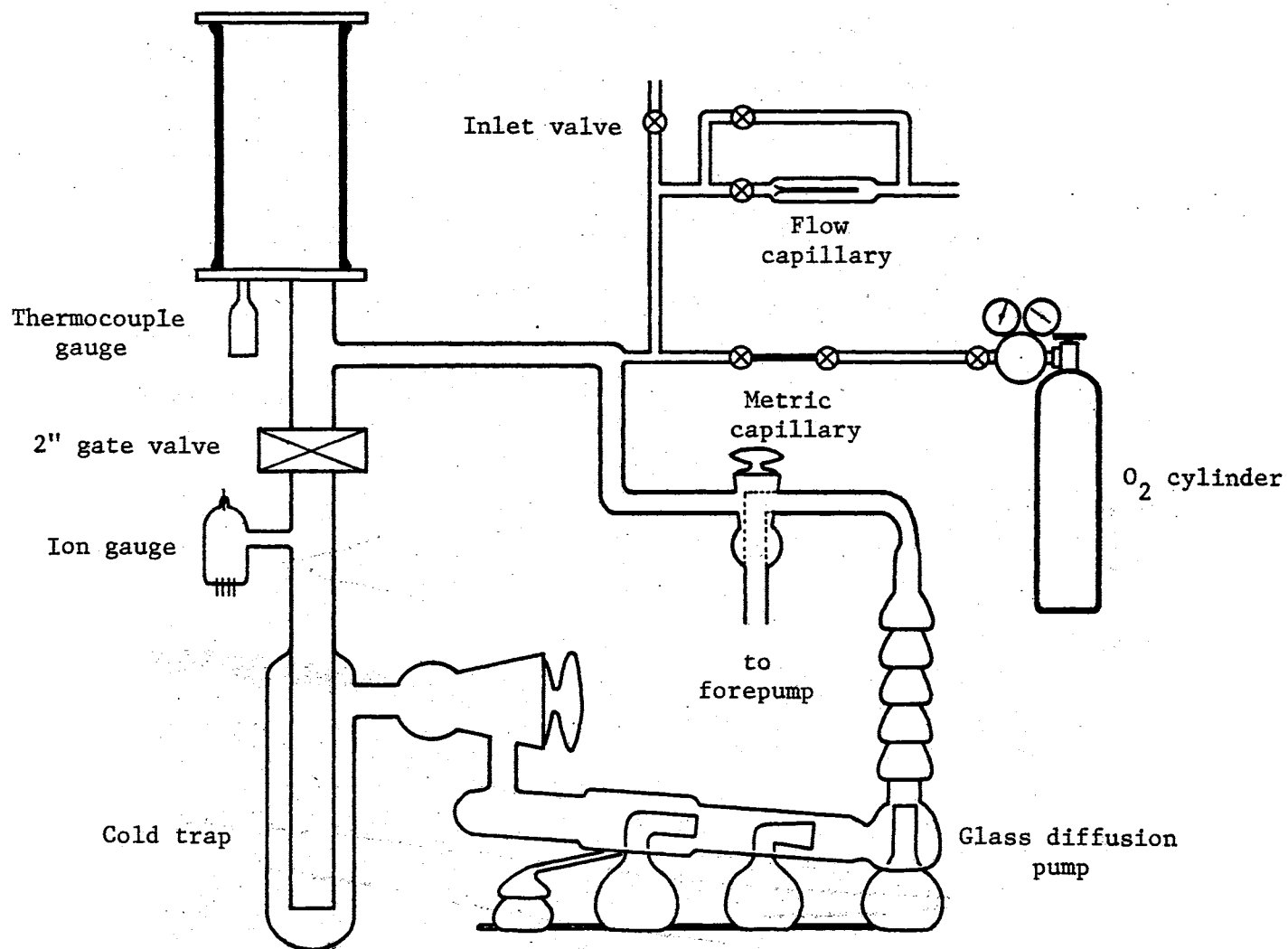


Figure 2. Diagram of Vacuum and Gas Handling System

all of the tunnel junctions used in this study, are evaporated from the tungsten boat shown in the lower part of Figure 3. The uncertain evaporation rate during heating and cooling of the boat is avoided by shuttering the vapor except for timed intervals when the boat temperature has stabilized. The usual evaporation rate is approximately $80\text{\AA}/\text{sec}$.

The other metallic films are evaporated from the filament, usually tungsten, which is supported from the upper plate of the vacuum chamber. Because of the low current capability of the feedthroughs, the filament is small and therefore the amount of material which can be evaporated is restricted to a few milligrams. The small charge and the lack of shutter between the substrate and the filament necessitate degassing below the melting point of the charge and the actual evaporation is performed within 1 to 10 seconds depending on the charge size. During this rapid evaporation the system pressure may rise to 10^{-5} torr. The table lists details of standard evaporation procedures.

Both evaporation sources are well shielded to reduce the plating of other parts of the chamber, and contamination of subsequent films. There have been no measurable effects of the contamination of Pb·I·Pb junctions with Fe although the Fe may have been evaporated immediately before the Pb.

The molybdenum masks which define the metallic stripes are held by a rotating platform which has room for five masks. The proper mask is selected by rotating the iron mask control rod with a permanent magnet and the platform being fastened to a common shaft rotates also. Spring tension holds the mask in position during evaporation.

A number of masks producing a range of stripe widths from 0.127 mm to 1.6 mm have been used. Another set of masks produces films with two

TABLE I

STANDARD EVAPORATION PROCEDURES

Material Evaporated	Source	Power	Notes
Pb: Marz grade Pb from Materials Research Corp, severely etched in a mixture of equal parts hydrogen peroxide and glacial acetic acid. A slight amount of acetic acid in the rinse prevents build up of scale which covers the surface of the molten charge.	boat: $\frac{1}{2}$ " x 4" x .005" hot zone diple tungsten boat from R.D. Mathis Company.	18 VAC (variable transformer setting) 3.5 - 4.2A to primary of current transformer.	Degass at same power level with shutter closed.
Fe: 0.005" 99.995% Fe wire from Alfa or #36 Standardizing wire from J. T. Baker.	filament: Three 0.010" tungsten wires twisted together or one 0.020" tungsten wire.	65 VAC approx. 1.0A to primary of 6.3 V, 18A filament transformer.	Degass at 0.6A, approx. 35 VAC. Switch power on quickly and off after minimum evaporation time to reduce heating effects.
Ni: 0.005" 99.97% from Alpha.			

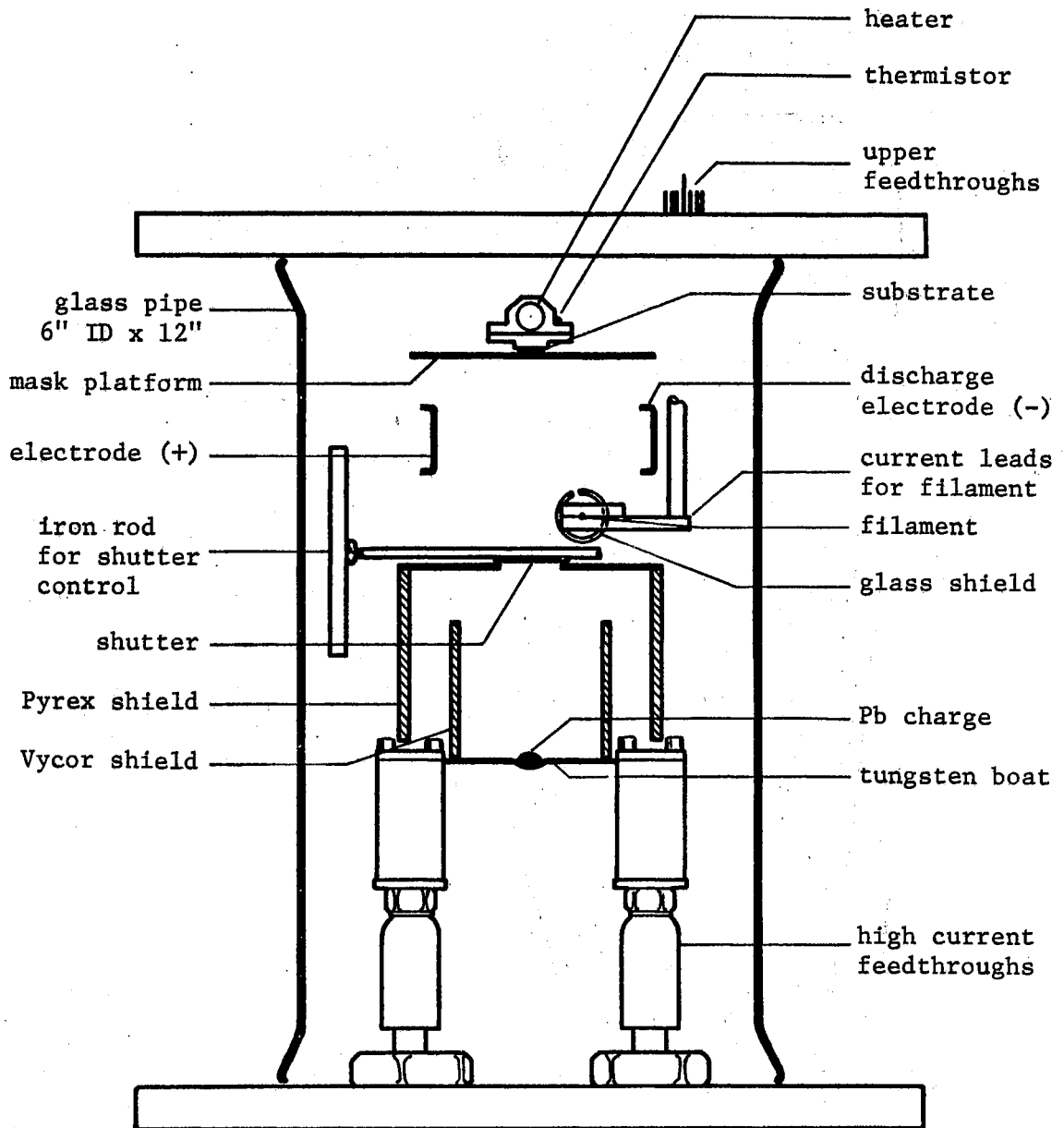


Figure 3. Evaporation Chamber

of the cross stripes oriented at $\pm 45^\circ$ angles from the long stripe and arranged to intersect within the area of the long stripe. These cross stripes are evaporated at different times to form a three layer sandwich with two junctions on either side of the long stripe and no direct tunneling between the cross stripes. The third cross stripe has the same configuration as those in Figure 1, and is formed simultaneously with one of the angled stripes.

Film Thickness Measurement

An optical interference technique is used for absolute thickness measurement. A half-silvered proof plate is placed within a few optical wavelengths to the film and is illuminated with monochromatic light. Interference between the light reflected from the proof plate and that reflected from the film produce light and dark bands across the surface. The resultant pattern is a contour map of the film surface with each fringe representing an additional separation of the film and proof plate by one half wavelength of the illuminating light. The thickness of the film can then be measured by comparing the displacement in the fringe pattern at the film edge to the separation of the fringes. Since there is a change in phase upon reflection of light from surfaces which is dependent upon the nature of the surface, the film edge which is to be measured should be overlaid with another film to avoid false shifts due to the difference in reflected phase between the film surface and the underlying surface. This requirement is relaxed for large fringe shifts and for the cases when the measured film and the underlying film are the same material.

A Unitron BMEC microscope with interference accessories is used to

produce Polaroid photographs of fringe patterns with 6440\AA light which is transmitted through an interference filter. The fringe separations and displacements are measured from the photograph. If a precision much less than one hundred Angstroms is required, constant density contours may be plotted from the photograph and the fringe shift measured more accurately than with "eyeball" determinations. The Unitron microscope is used as a diffuse reflecting densitometer by eliminating specular reflection with crossed polarizers and mounting a photodiode on one of the eyepieces. The objective power and the field stop of the Kohler illumination system determine the area sampled for the density measurement. Figure 4 shows constant density contours of a 98\AA Fe film with Pb overlay; the step in the fringe pattern is well resolved. An optimum spot diameter seems to be 0.4 mm which is just large enough to average over the film granularity.

For films so thin that the interference technique is no longer useful, another thickness calibration is used. The mass of the film deposited on the shield surrounding the tungsten filament is measured by weighing the shield both with the film and after etching the film away. A Mettler M5 microbalance having a reproducibility on the order of 10 micrograms insures one percent resolution on all of the films thicknesses encountered in this study. The calibration between sample film thickness and shield film mass has been determined with sample films thick enough for good interference determination and is $58\text{\AA}/\text{mg}$ for Fe.

Oxidation Techniques

The insulating barriers in tunneling junctions have been produced by forming monolayers of organic molecules, polymerizing molecules and

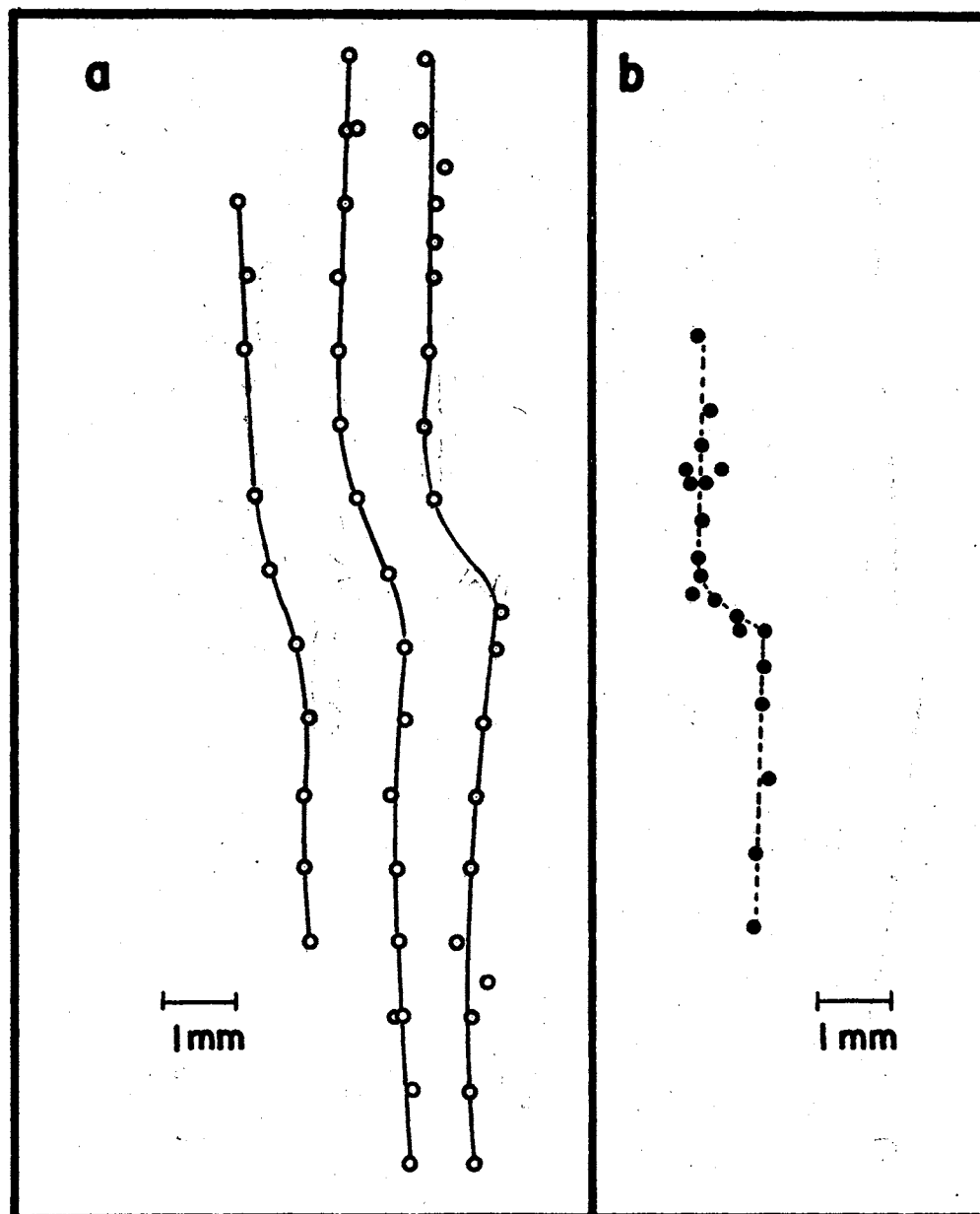


Figure 4. Constant Density Contours of the Fringe Pattern of a 100\AA Step in Film Thickness. a) 0.4 mm scanning spot diameter, b) 0.1 mm scanning spot diameter. The fringe separation corresponding to 3220\AA is 29.5 mm .

evaporating layers of inorganic compounds, but the most common techniques involve some method of oxidation of the metallic films, such as exposure to air, heating in air or oxygen or exposure to a glow discharge in a low pressure oxygen atmosphere (13, 84). The primary method chosen was the glow discharge oxidation since the method introduces fewer contaminants.

Oxygen is admitted to the vacuum system to a pressure of 50 - 300 microns of Hg, a high voltage discharge is initiated and the ionized oxygen atoms are allowed to fall upon the surface of the film. The process requires only a few seconds, the exact oxidation time depending upon the gas pressure, the discharge current, and geometry, and the tunneling resistance desired.

There has been an evolution of the discharge electrode configuration as problems have arisen in the oxidation process. The first electrode was a stripe of Pb foil wrapped around a circle formed of glass rod and suspended in the vicinity of the present electrode location (see Figure 3). The negative terminal of the high voltage was connected to the electrode and the positive terminal to the upper chamber plate. The barriers formed with this arrangement showed shorts and excess currents and other signs of non-uniform barriers as is discussed in Chapter III, with a marked increase in such symptoms with increasing discharge voltage. The hypothesis being that high energy ions damage the extremely thin oxide layer, an electrode arrangement to shield the film from ions in direct paths from the electrode was made by wrapping the electrode foil outside a glass cylinder which served as the shield. There was a significant reduction in apparent inhomogeneities with this geometry.

When sputtering of iron was attempted, the need for more electrodes and good shielding between them forced another change in the electrode design. Oxidation electrodes were lead or aluminum, chosen for its low sputtering rate, wrapped around glass tubes and inserted in slotted aluminum or stainless steel tubes. The diameter of the tubes was chosen to insure that the distance between the electrodes and the grounded tubes was always smaller than the cathode dark space for all discharge conditions anticipated, and thus to prevent discharge or sputtering from any part of the electrode except at the tube slots (141). The sputtering electrodes of iron were the same design. This design gave variable results for oxidation of Pb films. Excess currents were still present in many films, while some showed ideal characteristics. The exposed iron electrode was subject to secondary sputtering, a visible deposit forming on a piece of microscope slide placed near the electrode during one test discharge. The deposit no longer appeared when the iron electrode was grounded.

During tests to determine causes for the variability of oxidation results, much attention was given to impurities in the oxygen atmosphere. Variations in the composition of the component gases were detected qualitatively by spectral means. A 15,000 line/inch diffraction grating was taped in front of the lens of a Polaroid 110A camera, and the discharge photographed through a slit. The image of the slit and the spectrum then appear on the resulting print as shown for two cases in Figure 5. The impurity lines visible in the figure were reduced by flowing the oxygen and pumping continuously, or by cooling the oxygen line with liquid nitrogen, by leaving the nitrogen trap open to the system and closing off the diffusion pump. Since the contaminants are pumped by

liquid nitrogen chilled surfaces, water in the oxygen and adsorbed upon surfaces is thought to be the primary constituent. As a standard procedure the surfaces are cleaned by a predischARGE at much higher currents than oxidation. If the contaminants are still coming from the surfaces as indicated by a change of color of the positive column from the normal yellow green of the pure gas discharge to a bluish color, the gas is pumped off and the process is repeated until the pure color remains as long as the expected oxidation period.

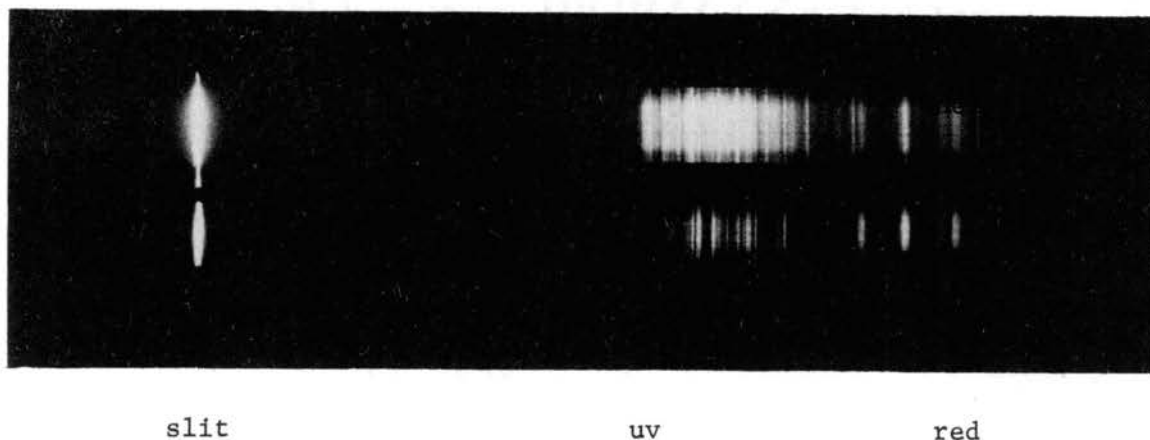


Figure 5. Spectra From Glow Discharge With and Without Contaminant Lines Visible

The electrode design in Figure 3 is the result of an effort to reduce shorts and inhomogeneities further and increase the consistency of the tunneling characteristics. The mask holder which surrounds the film is grounded to the upper chamber plate which served in the previously discussed designs as the positive electrode. Since there is a e.m.f. difference measured to be 10 - 20 volts between the positive column of

the glow discharge and the positive electrode, there is a relatively high electric field in the immediate vicinity of the positive electrode and therefore the film which is being oxidized (142). Thus negatively charged particles could be accelerated to an energy of several eV before colliding with the surface of the oxide, possibly damaging it. With the positive electrode separated from the ground plate, the potential of the top plate floats about 20 volts negative with respect to the positive electrode and the resulting junctions show no excess current and very nearly ideal characteristics similar to those produced by thermal oxidation.

Thermal oxidation proceeds in an atmosphere of oxygen at atmospheric pressure and at elevated substrate temperatures. After evaporation of the one Pb film, the vacuum chamber is filled with oxygen and a flow is established from the oxygen tank out through the upper plate seal. The substrate is brought quickly to 50°C by applying 120 VAC to the substrate heater, after which the substrate heater voltage is reduced to 24 VAC and the temperature as detected by the thermistor stabilizes very near to 50°C. The film is held at that temperature for enough time to produce the desired junction resistance: approximately 1.5Ω for 1 mm² junction and 3 hour exposure, the resistance increasing roughly as the square of oxidation time. At 100°C the oxidation time is reduced about a factor of ten. After the heater is turned off, the substrate is allowed to cool about 3 hours to 30 - 33°C before the oxygen flow is stopped and the gas is pumped off. Pumpdown after thermal oxidation is very slow, usually 30 minutes to 1 x 10⁻⁵ torr, at which time evaporating some of the Pb charge will reduce the pressure quickly to 4-6 x 10⁻⁶ torr. The second layer of Pb is then evaporated.

The uniformity of resistance between junctions is very high with less than 20% variation between equal area junctions indicating that the uniformity within one junction should be correspondingly high. The interjunction resistance variation is much higher for glow discharge oxidation processes, due to the geometry of the plasma.

Tunneling Measurements

Current-voltage characteristics of junctions are measured with the apparatus diagrammed in Figure 6 by recording on a Moseley 135 X-Y recorder the direct current through the junction provided by the variable dc source and the voltage across the junction measured by a Keithley 149 electrometer. The Keithley electrometer allows usable full scale voltage recordings from 0.1 mV to 100 mV. The lower current range is limited by the recorder current sensitivity which is 0.5 μ A/inch (3.5 μ A f.s.). The current sensitivity is adjustable in a 1,2,5 sequence to 50 mA/inch. The dc source resistance is one ohm plus the lead resistance which is about two ohms.

The derivative dV/dI is measured by applying a small ac current of constant amplitude to the junction and monitoring the resultant ac voltage appearing across the junction. This signal is then proportional to the junction resistance at the dc bias point. The ac current source is transformer coupled in series with the low impedance dc source to maintain a high ac source impedance, which is nevertheless reduced by the presence of the inductive susceptance of the transformer secondary. This reactance is therefore resonated at the ac signal frequency with the capacitance to accomplish two purposes: raise the source impedance of the 990 Hz signal to near 200 k Ω and reduce noise and interference by

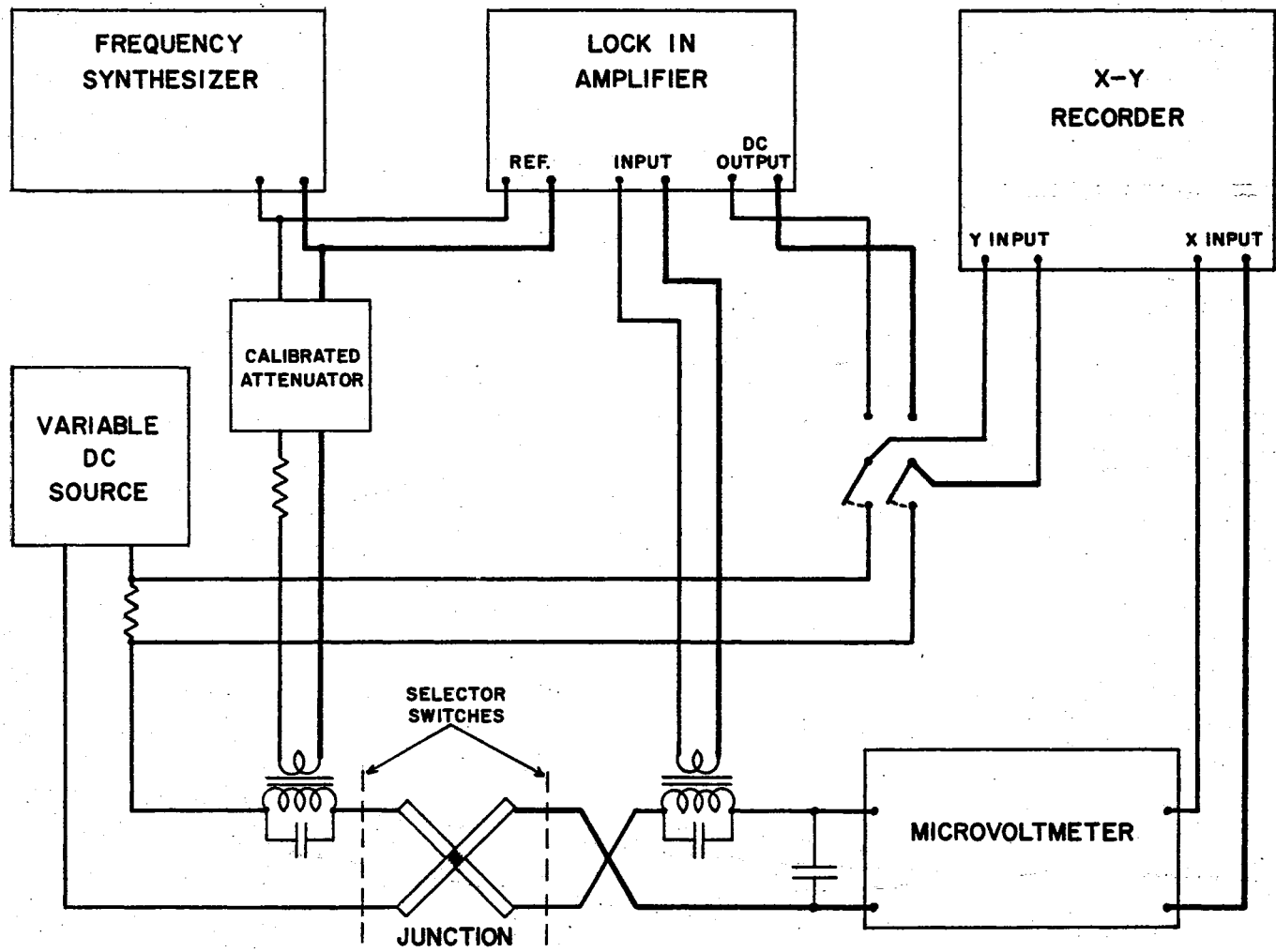


Figure 6. Circuit for Junction Testing

shunting the noise at frequencies away from resonance. The 990 Hz signal frequency was chosen to be between the 16th and 17th harmonics of 60 Hz.

The current and voltage pickoff transformers are toroidally wound high Q transformers with Q's near 200 at the 990 Hz operating frequency. Due to the high Q, stabilities of frequency, inductance, and capacitance are important to reduce phase shifts and resultant amplitude errors. Since the permeability of the transformer cores are temperature sensitive, the transformers are wrapped in high permeability shielding foil to reduce hum pickup, mounted with the resonating capacitors on a copper block, surrounded by copper sheeting and isolated by insulating supports within the chassis of the test circuit. With such precautions to reduce effects of ambient temperature fluctuations, there were still phase shifts of ten degrees over periods of 4 hours as measured by the PAR Lock-In Amplifier for the worst case condition of an open circuit, i.e., the effective junction impedance infinite.

The copper block upon which the resonant circuits were mounted was then temperature controlled by the circuit shown in Figure 7. The thermistor is the temperature sensor and is in a bridge arranged so that increasing thermistor resistance causes current flow in the 2N1724 transistor. This transistor is mounted directly on the copper block and is the heating element. The use of the transistor as the heating element rather than a resistor whose current would be controlled by the transistor results in a power dissipation which is directly proportional to the bridge unbalance rather than the square of the unbalance, and a greater sensitivity at small unbalance conditions. The 100 mfd feedback capacitor reduces the response speed of the circuit and stabilizes its operation. Without the capacitor the circuit oscillates at about 2 cycles

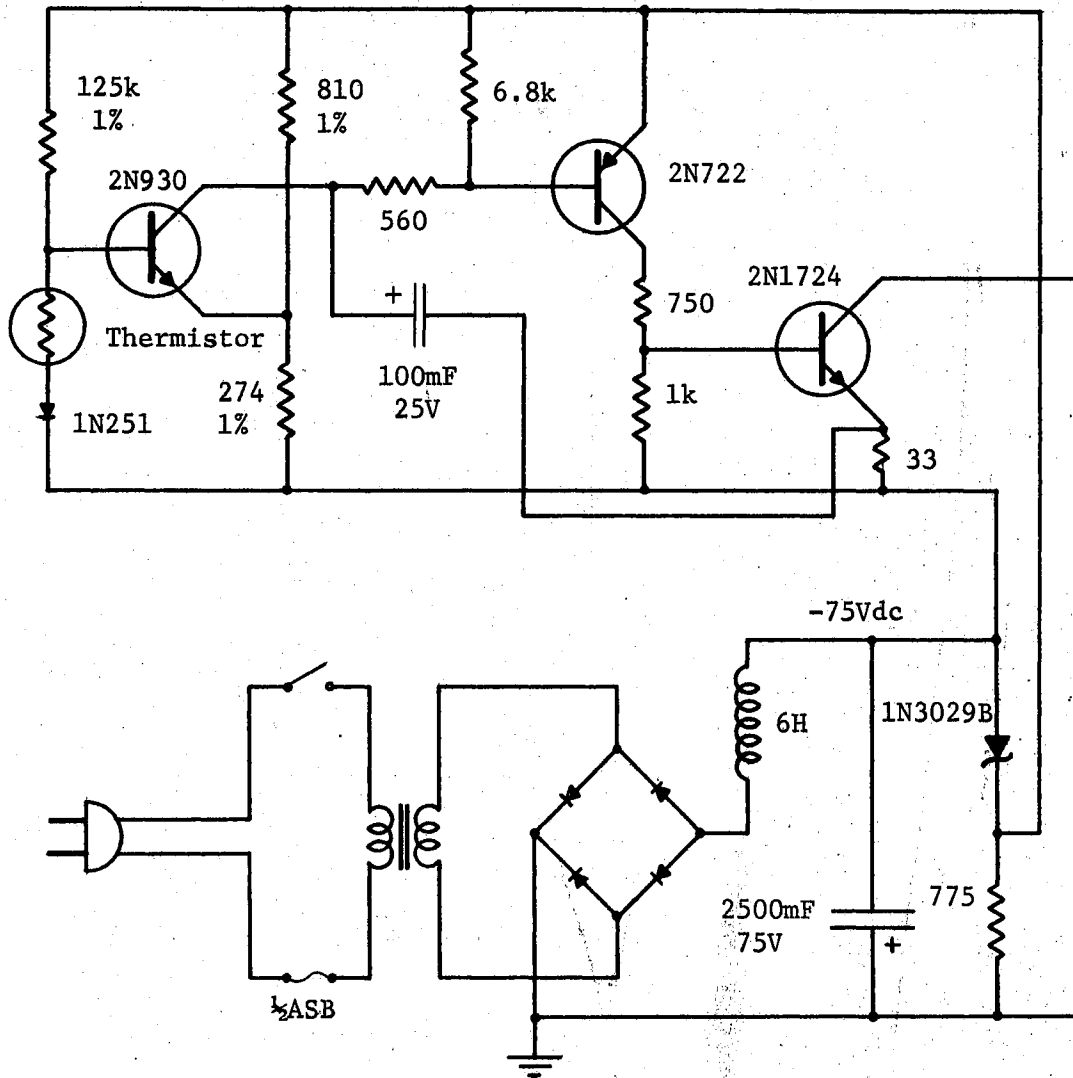


Figure 7. Circuit of Temperature Controller

per second when connected to the copper block. Short term fluctuations from the control temperature (nominally 30°C) are estimated by the heating current fluctuations and are found to be within 0.02°C .

The current-voltage characteristics of lower resistance junctions can be displayed on an oscilloscope with the circuit diagrammed in Figure 8. The resistance limit is determined by two requirements that the junction resistance be much less than 1) the current sensing resistor (10 ohms in the figure) and 2) the input impedance of the transformer which is 25 ohms shunted by frequency dependent reactances. The 25 ohms resistance is the reflected resistance of the $8\text{K}\Omega$ resistor in the secondary which was necessary to damp the resonance of the transformer and leads. The shunt inductance and capacitance of the transformer cause phase shifts and frequency dependent attenuations whose effect on the oscilloscope display can be minimized by optimizing the driving frequency and using the minimum current drive necessary for the particular observation of interest.

Thermal Environment

The tunneling junctions are tested at room temperature, in liquid nitrogen (77°K) and in liquid helium (4.2°K) during preliminary testing and in a pumped helium bath for the lower temperature measurements to 1.2°K . The sample holder, a photograph of which appears in Figure 9, is designed to be immersed in a liquid helium storage dewar to allow quicker measurements and more efficient use of liquid helium. The preliminary testing proceeds as follows: 1) measurement of stripe and junction resistance at room temperature, 2) immersion of the sample in liquid nitrogen and measurement of the same resistance, 3) quick transfer of the

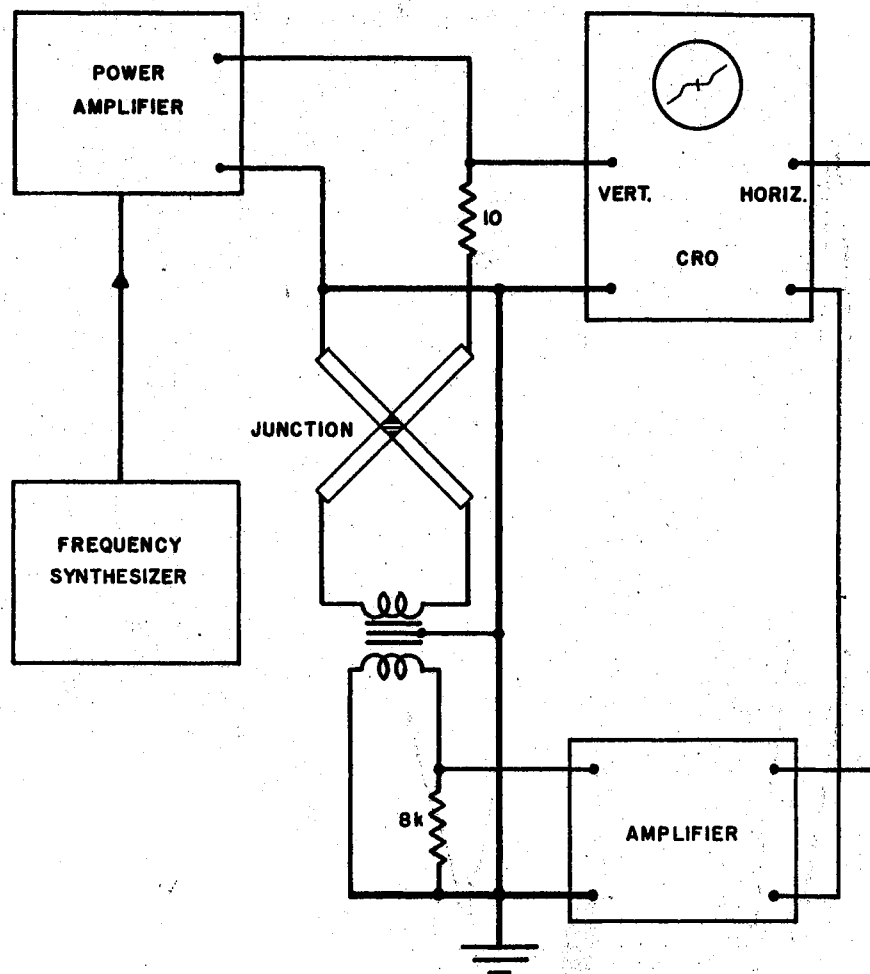


Figure 8. Circuit for Oscilloscope Display of Current-Voltage Characteristics

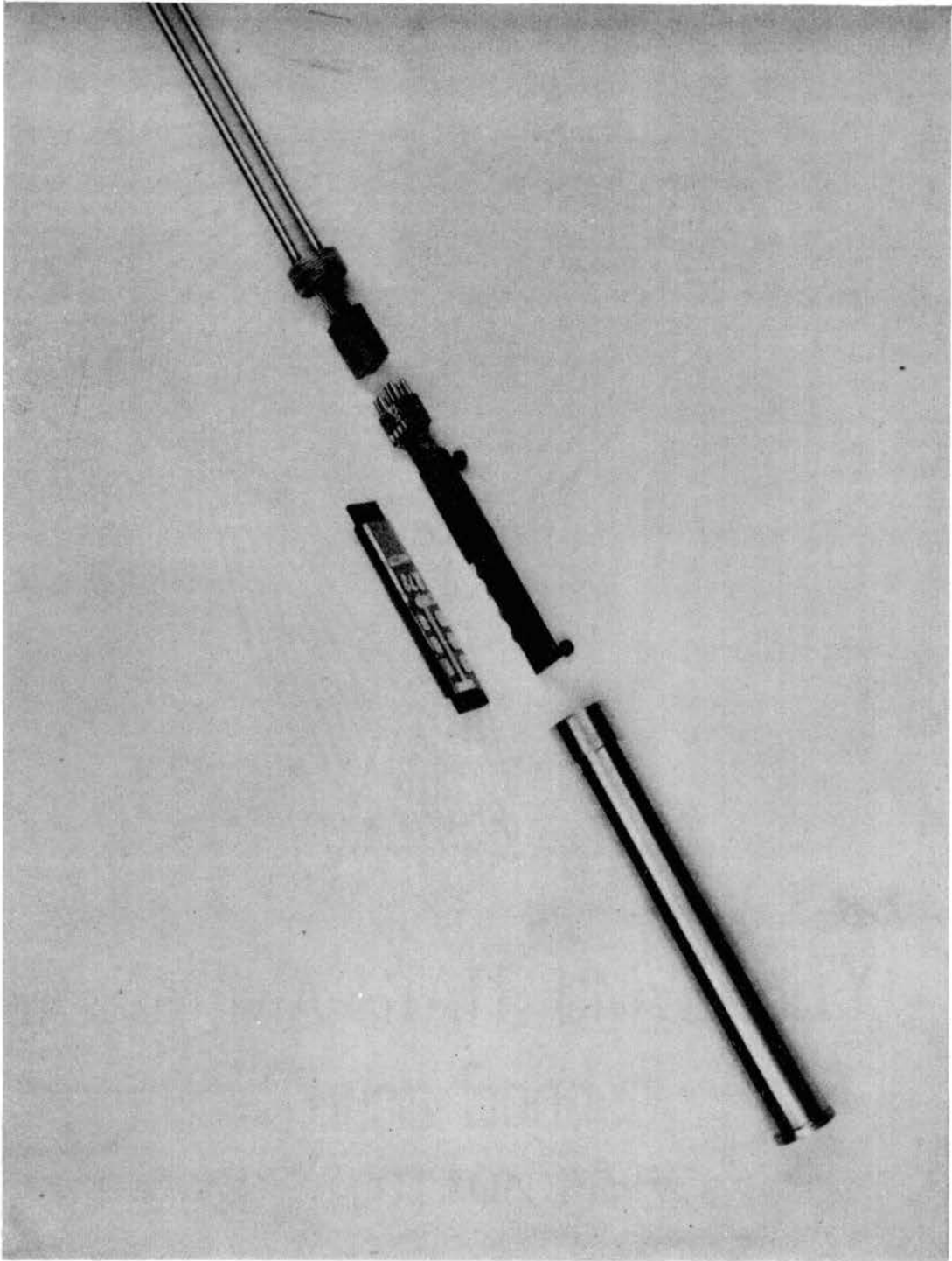


Figure 9. Photograph of Sample Holder

sample to the liquid helium storage dewar and plotting of current-voltage and derivative-voltage characteristics, 4) return to liquid nitrogen storage.

To obtain lower temperatures the helium bath in the dewar system (Figure 10) is partially evaporated by a vacuum pump thus cooling the bath. With a Precision Scientific 1000 pump the lowest bath temperatures lie between 1.3° and 1.2° Kelvin as measured by the helium vapor pressure. Because of the thermal conductivity of liquid helium below the λ -point the temperature of the tunneling junctions be the same as that indicated at the surface of the bath by the helium vapor pressure (143, 144).

Magnetic Environment

Magnetic fields, may be applied either with the solenoid surrounding the sample or the 0-13kG electromagnet. When no fields are to be applied, the solenoid is removed from the dewar, the dewar system is swung away from the electromagnet and the magnetic shielding can is placed over the dewar to shield the earth's field.

Alignment of the sample with the field of the electromagnet is accomplished by reflecting the light beam from a laser off the surface of the slide. The laser itself is initially aligned by reflecting the beam back on itself from a mirror held at right angles to one of the magnet pole faces by a precision right angle block. For this alignment the magnet, which rotates on its base, is in the 90° position. The sample in the dewar is then substituted for the right angle reflector and is rotated until the light is again reflected back on itself. Because of refraction by the liquid nitrogen or liquid helium filled dewars,

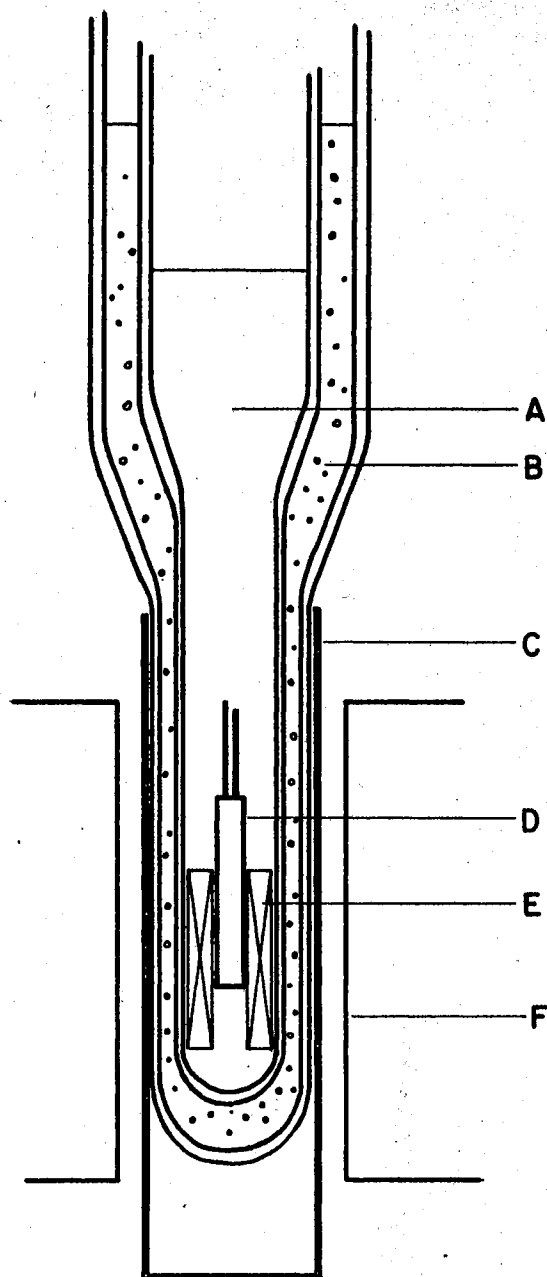


Figure 10. Dewar and Magnet Systems. A) Liquid helium, B) liquid nitrogen, C) magnetic shield, D) sample can, E) solenoid, F) pole face 0-13kG magnet.

the angle at which the light strikes the dewars should be normal to the surfaces and can be checked by observing the rather broad reflection from the curved and more irregular dewar surfaces. When the sample is inside the solenoid and the film is not visible, the beam is reflected from a flat on the solenoid which is in turn aligned with the sample slide by a tongue which slips between the two sides of the sample holder just below the sample.

The magnitude of the magnetic fields are determined for the two magnets by different methods. The large electromagnet field is measured by a rotating coil gaussmeter and the solenoid field by measurement of the solenoid current and field calculation from the solenoid geometry.

By treating the solenoid as a collection of single turn loops, integrating over the winding volume, and keeping the lowest order terms in radii to length ratios, one finds that the axial field can be written as

$$B_{\text{axial}}(Z) = \frac{\omega_0 n I}{\ell} \left[\left(1 - \frac{a_1^2 + a_1 a_2 + a_2^2}{12} \right) \left(\frac{1}{\left(\frac{\ell}{2} - Z\right)^2} + \frac{1}{\left(\frac{\ell}{2} + Z\right)^2} \right) \right]$$

where a_1 and a_2 are the inside and outside radii of the solenoid, ℓ is its length and Z is the distance away from the center along the solenoid axis. The effect of the correction terms in the equation is to reduce the solenoid sensitivity from the 5.277 G/mA value for an infinite solenoid to 5.06 G/mA at the center and 5.05 G/mA 0.2 inches away from the center, the approximate locations of the three junctions in the configuration of Figure 1 when the sample is inside the solenoid,

CHAPTER III

TUNNELING IN Pb-I-Pb JUNCTIONS

Single Particle Tunneling Effects

A comparison of tunneling between superconductors and between normal metals reveals the striking difference in Figure 11(a). Here the current voltage characteristics of a lead-lead oxide-lead junction at 4.2°K in the earth's magnetic field and in a field large enough to destroy the superconducting state clearly show the effect of the superconducting energy gap which had been measured only indirectly through heat conductivity and specific heat experiments before use of tunneling measurements (145, 146). The sharp increase in conductivity near 2.6 mV reflects the very high density of superconducting states at the band edge, which is in qualitative agreement with the weak coupling limit theory of BCS (19) who predict a square root discontinuity in the density of states of the form $N(0) \frac{E}{|E^2 - \Delta^2|^{1/2}}$, where $N(0)$ is the normal metal density of states at zero temperature, ϵ is the energy per electron measured from the Fermi level and Δ is the energy gap parameter. The pair tunneling current at zero bias is not visible in this plot.

The tunneling experiment can be easily visualized by the semiconductor model of Figure 12. The ground state of the superconductor has all of the pair states below the energy gap filled and all of the excited states above the gap empty. At temperatures above 0°K single

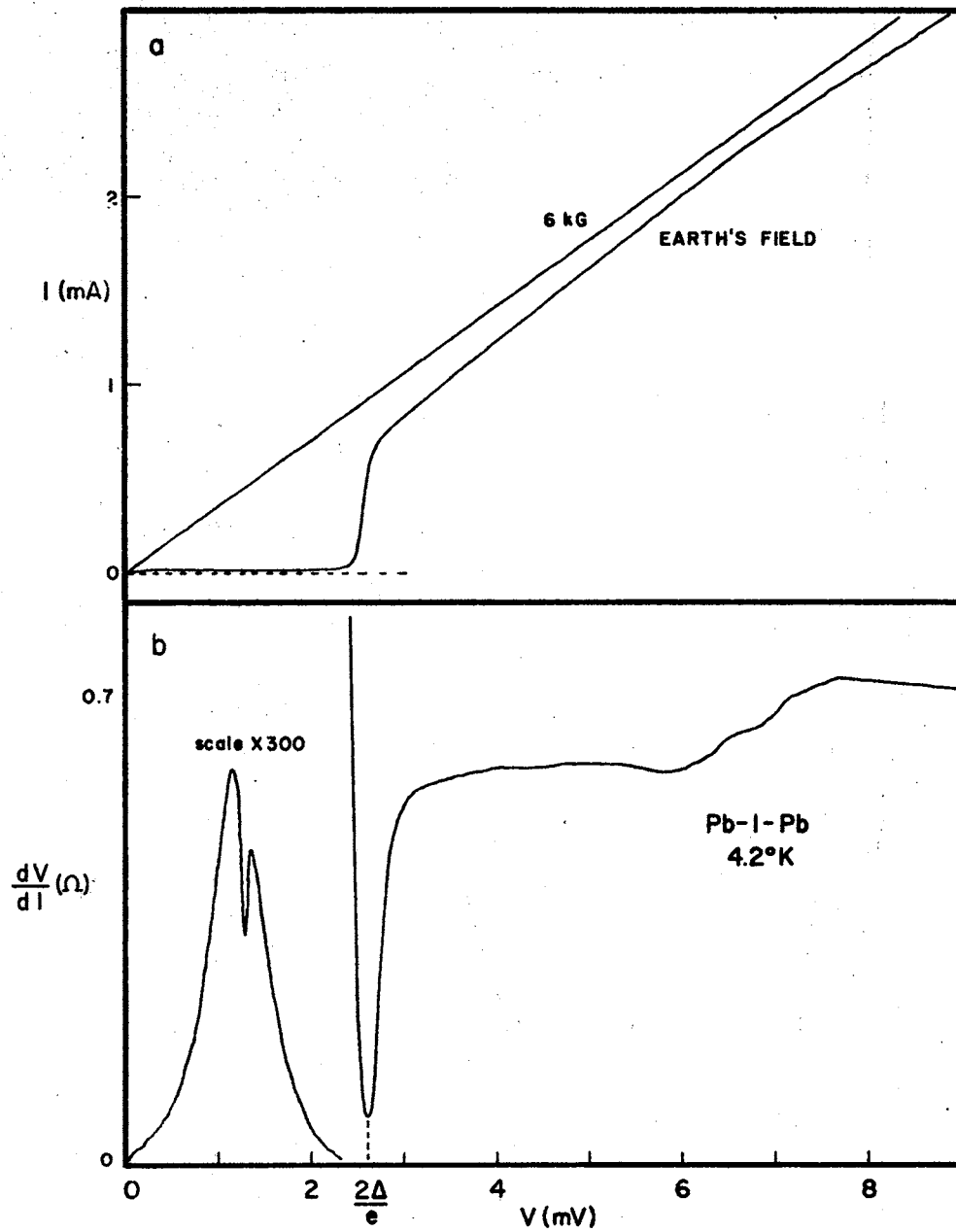


Figure 11. Current and Derivative Characteristics of a Pb-I-Pb Junction at 4.2°K

particles are thermally excited according to Fermi-Dirac statistics, above the gap leaving behind vacant pair states.

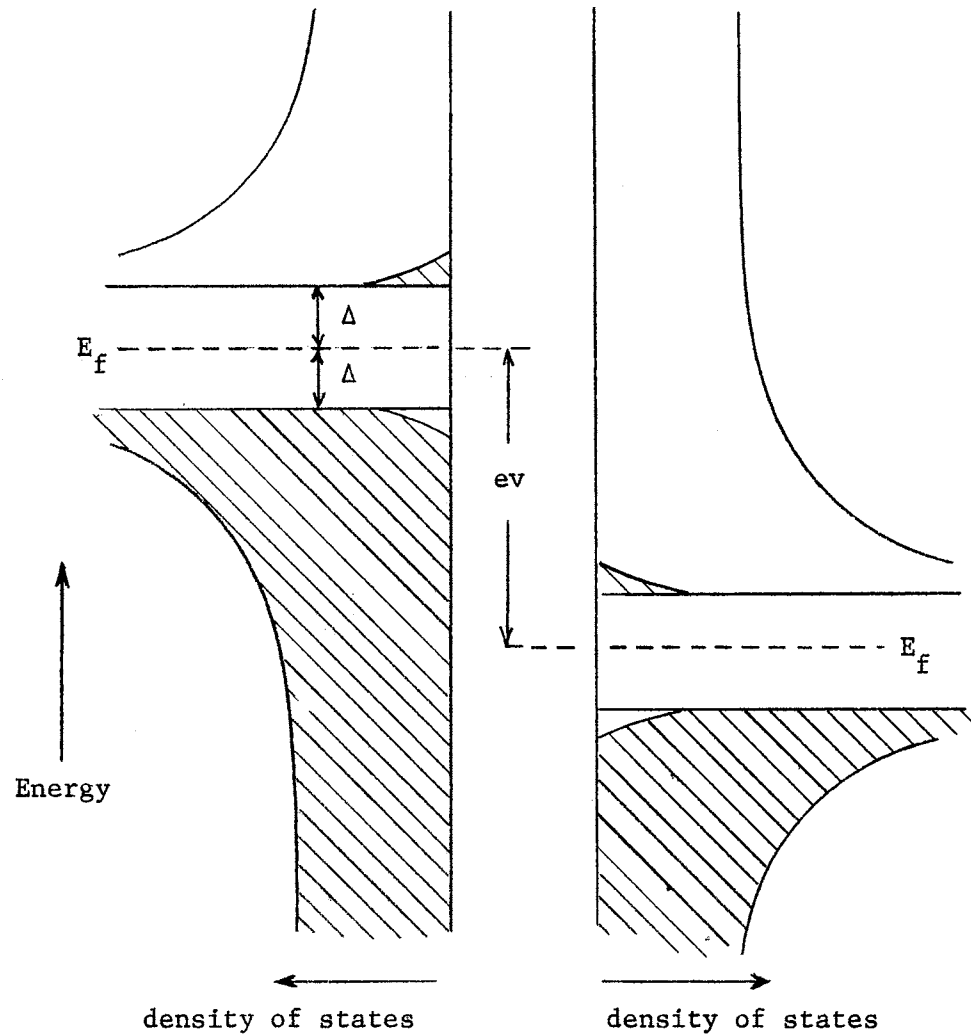


Figure 12. Semiconductor Model of Tunneling Experiment

When the relative energies of the states on the left are increased by application of an emf between the superconductors, equilibrium is disturbed and a tunneling current appears which depends upon the number of available particles and vacant states and the matrix elements between

the initial and final states.

As the junction bias is increased from zero, the current, initially due to thermally excited single particles and to lower probability pair tunneling mechanisms, is small. But when the bias is increased so that $eV = 2\Delta$, direct tunneling from the dense pair states into the equally dense excited states at the band edge becomes possible and the current suddenly rises in the sharp step which is the distinguishing feature of superconductor-superconductor tunneling. With further increases in voltage more of the vacant states on the right become available and the characteristic looks ohmic.

The semiconductor model as used does not include a means of handling momentum of the tunneling particles. This is not a serious hindrance as conservation of energy is the most important consideration in superconducting tunneling experiments since a good accounting of the energy in the tunneling process, whether a photon or phonon is radiated or absorbed or whether the tunneling is elastic, is sufficient for description. Momentum and energy cannot simultaneously be conserved in elastic tunneling except in special cases and, since the momentum of an electron in a solid is only defined in the bulk for a given set of interaction with the lattice and other electrons, it is not surprising that momentum conservation is unimportant through a tunneling barrier which is laden with surfaces.

That the currents at junction voltages less than $2\Delta/e$ are due primarily to thermally excited particles is demonstrated in Figure 13, where the low voltage region of a sample at 4.2°K and 1.7°K are compared. A rough estimate of the amount of current due to thermally excited single particles can be made by approximating the density of states of the

superconductor as two narrow bands on either side of the gap. This is not a bad approximation because of the relatively high density of states near the band and the exponential decrease of excited states away from the band edge. The ratio of excited state current to the current at voltages just above the band edge at 4.2°K for a half gap of 1.3 meV should by this model be 0.028 . The measured ratio, which is very consistent between films without excess currents, is $0.026 - 0.031$ depending upon the exact point on the knee of the I-V curve which is designated as the step height.

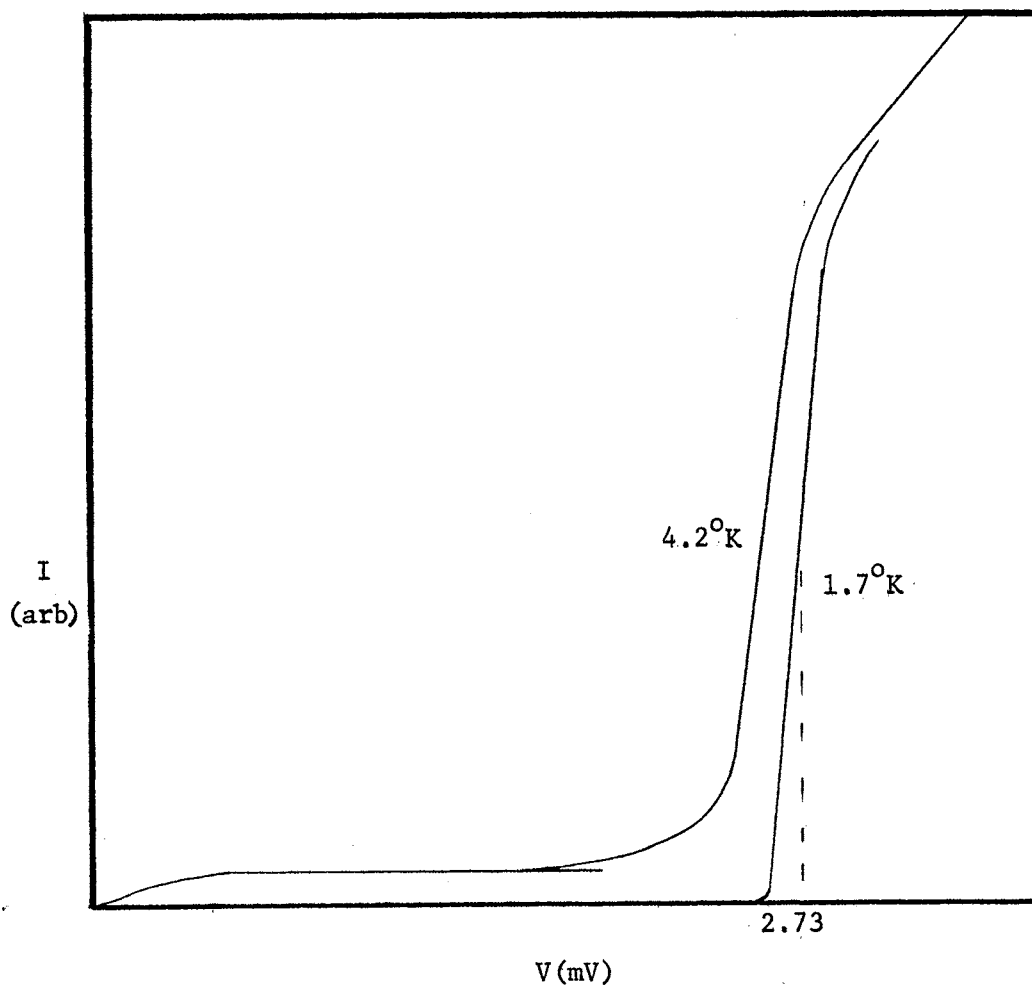


Figure 13. Temperature Variation of Low emf Tunneling Current

The derivative dI/dV is a good representation of the density of states as a function of energy since as the junction bias is increased a small amount δV , the tunneling current increases an amount δI which is proportional to the number of vacant states in the energy band $e\delta V$ at the energy $E = eV$.

There are other contributions to the derivative due to variation of the density of pair states away from the band edge in the superconductor from which the tunneling particles originate, but these variations produce smaller and more gradual changes in the derivative because the density of states change across the band edge is much larger and sharper. If an accurate measure of the density of states is desired, it is necessary to use a normal metal as the particle source, since the density of occupied states in the normal metal is reasonably constant up to the Fermi level. The resolution at any given temperature is reduced since the thermal spread at the Fermi level in the normal metal is not reduced by the presence of a superconducting gap.

Although the derivative dI/dV is a desirable quantity to measure directly, it is experimentally more difficult to obtain so the quantity plotted as a function of junction bias in these experiments is dV/dI . The high resistance (low conductance) at low voltages, sharp low resistance dip at $eV = 2.64$ meV, and the approximately ohmic behavior above occur in Figure 11(b) much as would be expected. The minimum in the derivative can be used as a well defined measure of the energy gap.

One feature which is not explained by the simple model which has been discussed to the point is the structure around 7 mV. In Figure 14 an expanded plot of the derivative over a range up to 27 mV shows the predominant features induced in the density excited of states through

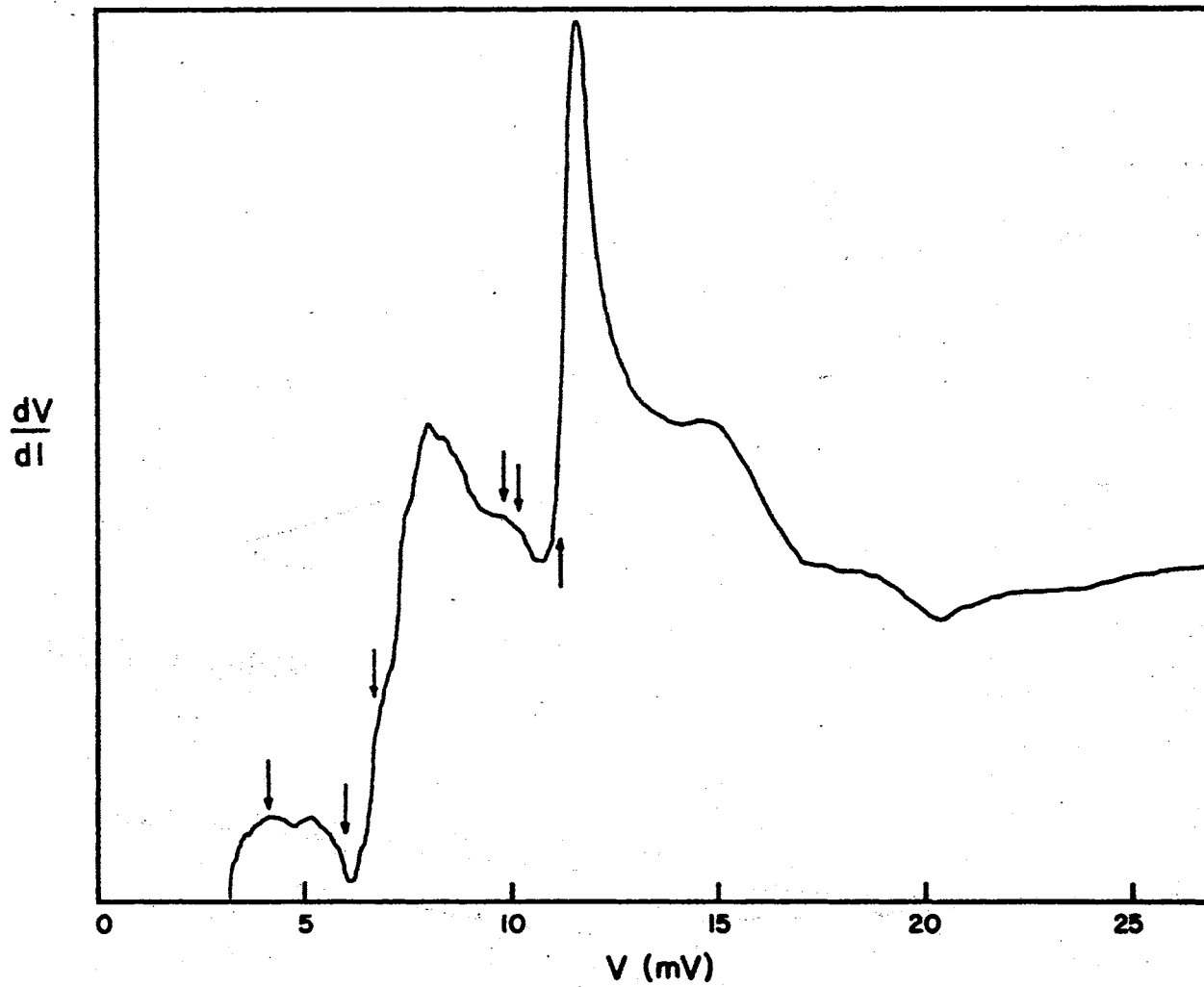


Figure 14. Expanded Derivative in the Region of Phonon Density Effects

the electron-phonon interaction. The energies of the peaks in the transverse and longitudinal phonon spectra of lead are 4.5 and 8 meV respectively and correspond well to the minima in the observed structure if energies are measured from $eV = \Delta$, i.e., the Fermi level of the superconductor into which the tunneling occurs. The electron-electron interaction which is responsible for pair formation and which is assumed small and instantaneous in the BCS limit, is neither for energy levels near the maximum energies of the lattice modes which participate in the attraction. This leads to an energy gap parameter which is complex and a function of frequency. The imaginary component of this parameter appears in the density of states as calculated by Eliashberg (31), giving rise to variations in the density of states as phonon densities vary. A full analysis is given in references 32 to 46.

This phonon structure is very reproducible between junctions, not varying with temperature in any significant way, and not varying with field except to be smeared as the edge of the energy gap is correspondingly smeared. This constancy should be expected from an effect which is controlled primarily by lattice vibrations being temperature and field insensitive.

Pair Tunneling Effects

The characteristic curves which have been discussed to this point have had pair tunneling effects suppressed or the sensitivities were not appropriate for their observation. There are three pair tunneling effects which can be easily observed in a superconductor-superconductor experiment and which will be discussed with particular reference to the detailed information about the tunneling junction which they can give.

These effects are: Josephson current, Fiske modes and subharmonic structure.

Josephson Current

Josephson's (52) theoretical prediction of a tunneling supercurrent arose out of extending the long range order of the superconducting state over a weak link, such as a tunneling junction. It is necessary for an understanding of Josephson's concepts to have an acquaintance with what is meant by long range order in the superconducting state and how it is described. The Meissner (147) effect of expulsion of magnetic fields from superconductors was strong evidence that the superconducting phase was a unique state that extends throughout the material. The macroscopic electromagnetic equations of the Londons (148, 149) which described the Meissner effect and the fact that magnetic fields actually do penetrate the superconductor a characteristic distance λ , 3.9×10^{-6} cm for lead as measured by Lock (150), indeed regarded the material as completely normal or completely superconducting. Since the intermediate state had been observed in which some regions of the superconductor were in the normal state and adjacent regions were in the superconducting state, a limit on the extent of the superconducting phase was necessary. This limit appeared in the Ginzburg-Landau (151) theory in which a spatially dependent, complex order parameter $\Psi(\vec{r})$ was defined so as to be analogous to a wave function for superconductivity, with the absolute square $|\Psi(\vec{r})|^2$ equal to the superfluid density of the two fluid model of superconductivity. The imposition of gauge invariance upon the supercurrent expression written in terms of $\Psi(\vec{r})$ leads directly to the London penetration depth when the system free energy is minimized. The magnitude of

the gradient of Ψ is limited to the order of $1/\xi$, thus guaranteeing a long range order which is limited in extent to ξ , the coherence length.

Josephson assumed that the phase ϕ of the complex order parameter Ψ which obeys

$$\frac{\partial \phi}{\partial t} = - 2\mu\hbar \quad (1)$$

where μ is the chemical potential, is coupled across a weak link in such a manner that gauge invariance is preserved:

$$\Delta\phi = \phi_2 - \phi_1 - \frac{2e}{\hbar c} \int_1^2 \vec{A} \cdot d\vec{r}$$

where 1 and 2 indicate adjacent points on opposite sides of the link, and \vec{A} is the electromagnetic vector potential. It is this last term which is responsible for the magnetic field effects. The result is the prediction of a dc supercurrent which is proportional to the $\sin \Delta\phi$,

$$J_s = J_o \sin \Delta\phi$$

where the spatial variation across the tunneling junction is given by

$$\nabla^2 \phi = \frac{1}{\lambda_J^2} \sin \Delta\phi$$

The quantity λ_J , called the Josephson penetration depth, is the characteristic distance which a magnetic field penetrates into the barrier region and is given by

$$\lambda_J = \left(\hbar c^2 / 8\pi e d J_o \right)^{1/2}$$

where d is the barrier thickness. And J_0 is given by

$$J_0 = \left[\frac{\pi \Delta(T) \sigma_{NT}}{2e} \right] \tanh [\Delta(T)/2kT],$$

σ_{NT} is the normal tunneling conductance per unit area, and k is the Boltzmann constant. [According to Fulton and McCumber (63) strong coupling effects in Pb will reduce the maximum current to 78.8% of the weak coupling limit.] The integral of J over the junction area gives the total supercurrent through the junction which in the limit of junction dimensions small with respect to λ_J , gives a diffraction-like dependence upon applied magnetic field,

$$I_s = I_0 \left| \frac{\sin \pi \Phi / \Phi_0}{\pi \Phi / \Phi_0} \right|$$

where Φ is the magnetic flux in the junction, and Φ_0 is one flux quantum

$$\Phi_0 = \frac{ch}{2e} = 2.07 \times 10^{-7} \text{ G cm}^2.$$

Since a parallel magnetic field penetrates the superconducting film on either side of the barrier an effective distance λ , the flux in the barrier is

$$\Phi = H w (2\lambda + d),$$

and the periodicity of the diffraction pattern gives a measure of λ , being on the order of hundreds of Angstroms while d is on the order of tens of Angstroms.

However, when the junction dimensions are no longer small, the self fields of the supercurrent tend to exclude the tunneling current from

the center of the junction, until in the large junction limit the current decreases exponentially away from the edge with a characteristic length λ_J (152, 153). The result is a linear dependence of tunneling current upon field as is shown in Figure 15. Owen and Scalapino (151) write the initial dependence of supercurrent upon magnetic field for a simple model of two colinear strips separated by a tunneling barrier as

$$I_s/W = 4\lambda_J J_0 - (c/4\pi) H$$

where W is the length of the edge along which the tunneling occurs, and H is the field applied parallel to that edge. Comparing the well defined slope indicated by the arrow with that obtained from the above equation,

$$\frac{dI_s}{dH} = - \left(\frac{c}{4\pi}\right) W$$

one begins as the effective width .026 mm, about one fifth of the stripe width. Conceptually, one could proceed to calculate $\lambda_J J_0$ by using the zero field current. Since J_0 is determined by easily measured quantities, λ_J could then be calculated, from which the London penetration depth of the film could be obtained. However, that procedure does not seem to be justified until the reason that the apparent edge length is only one fifth of the actual length is resolved: whether variation of barrier thickness across the width causes variation in tunneling probability in which case the value used for J_0 would be wrong, or whether the colinear model simply does not give better precision for the cross configuration.

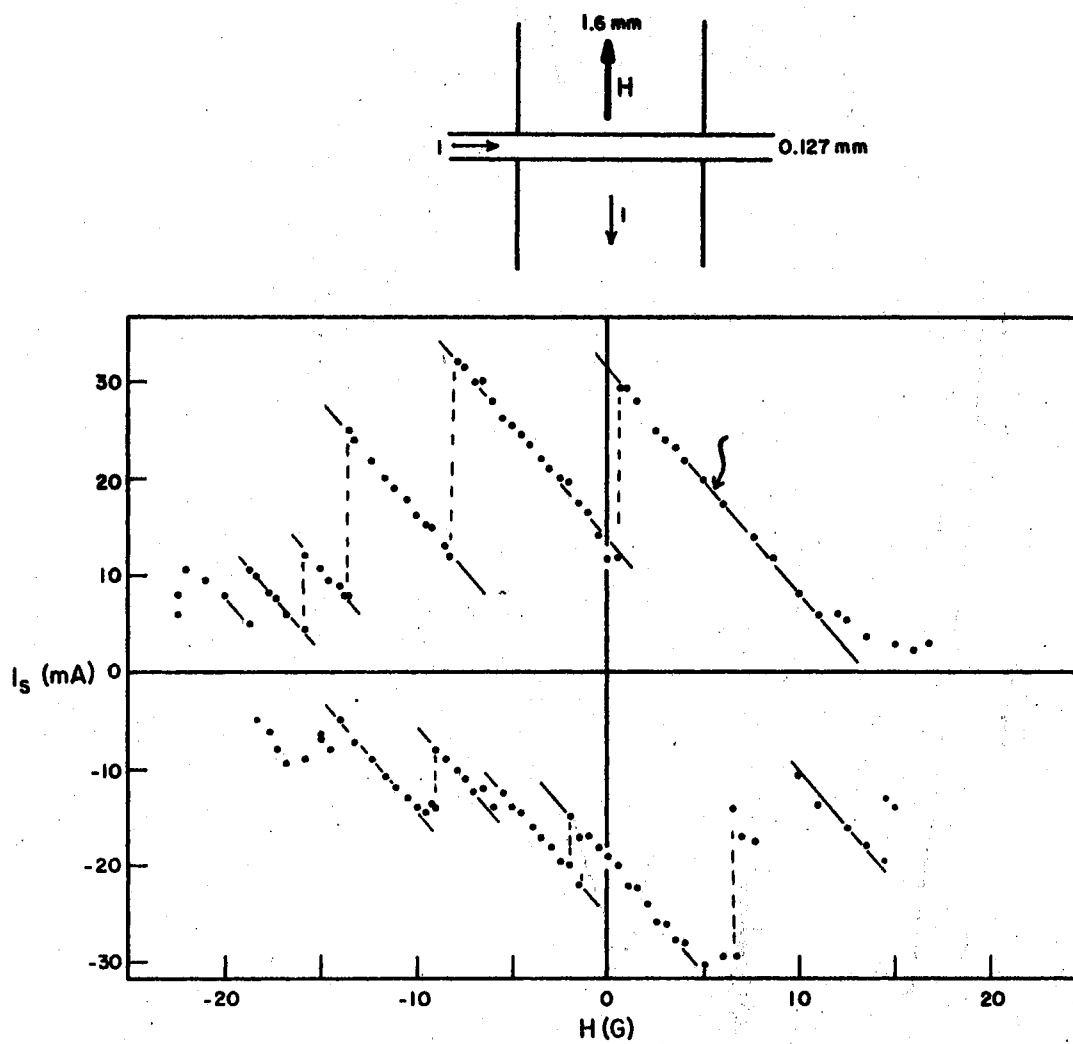


Figure 15. Magnetic Field Dependence of Maximum Supercurrent in a Low Resistance Junction

Fiske Modes

With application of an emf across the junction, the difference in Fermi levels produces a time varying phase difference according to Equation 1),

$$\frac{\partial(\Delta\phi)}{\partial t} = \frac{2(\Delta\mu)}{\hbar} = \frac{2eV}{\hbar}$$

and the current oscillates at a frequency $\omega = \frac{2eV}{\hbar}$. This is consistent with the fact that a tunneling pair must lose energy $\Delta E = 2eV$, which is radiated as a photon. The frequency of this radiation can be very high since the constant $2e/h$ is equal to 0.48 gigahertz per microvolt.

Evidence of the oscillating supercurrent is seen as steps in the I-V characteristic shown in Figure 16(a). These steps correspond to electromagnetic resonances of the tunneling junction as an open end strip line. The two sets of steps corresponding to resonant modes in the two different junction dimensions are not detectable in the I-V plot, possibly because one set is suppressed by the magnetic field (79). The second set does appear in the derivative plot in 16(b), where the decrease in resistance due to the narrow dimension resonances are indicated by arrows. The ratio of the average voltages between minima for the two sets is 0.0861, while the ratio of the nominal junction dimensions is close at 0.0795, so one can be assured that the proper dimension will be associated with a given voltage difference.

Coon and Fiske (79) gives the form for the electromagnetic wave velocity within the barrier as

$$v = \frac{c}{\sqrt{\epsilon} (2\lambda + d)/d}$$

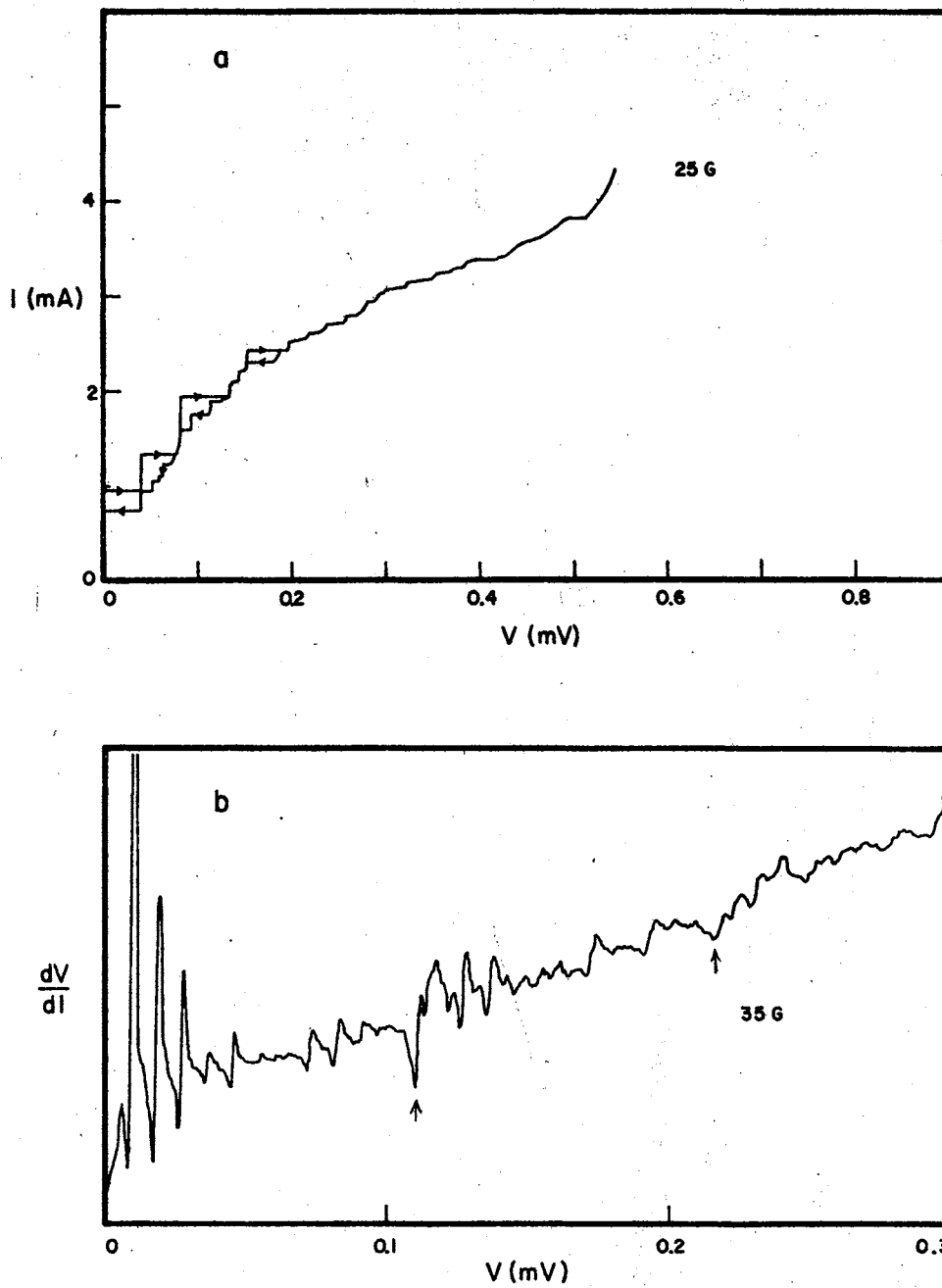


Figure 16. Fiske Modes Detected in the Characteristics of the Junction of Figure 15

where ϵ , the dielectric constant reduces the velocity in the same amount as in bulk materials, while the penetration of the magnetic field into the superconductor reduces the velocity by heavy inductive loading. Since the open end line has a resonance at each integral number of half wavelengths, the resonant frequencies are

$$\omega_n = \frac{n\pi v}{l}, \quad n = 1, 2, 3, \dots,$$

and since $2eV = \hbar\omega$, the ratio v/c is given by

$$\frac{v}{c} = \frac{2e(\delta V)l}{\pi\hbar c},$$

where l is the appropriate junction dimension, and δV is the emf difference between steps.

Because the tunneling probability is expected to fall off exponentially with d the barrier thickness, in analogy with simple barrier solutions, the tunneling resistance should be a sensitive measure of relative changes in d . To investigate the barrier thickness dependence in Fiske's velocity expression, the square of the ratio v/c is plotted as a function of junction resistance for several junctions in Figure 17. The legend indicates whether the junction is Pb-I-Pb or contains Fe, and whether the characteristics are ideal or show signs of excess currents. None of the junction types show any consistent dependence on the junction resistance. Representing the insulator as a square potential barrier of height eV_B and width d_e gives a junction conductance exponential in d for low tunneling probability,

$$\sigma_{NT} \propto \exp\left\{-\frac{1}{\hbar} (2meV_B)^{\frac{1}{2}} d\right\}.$$

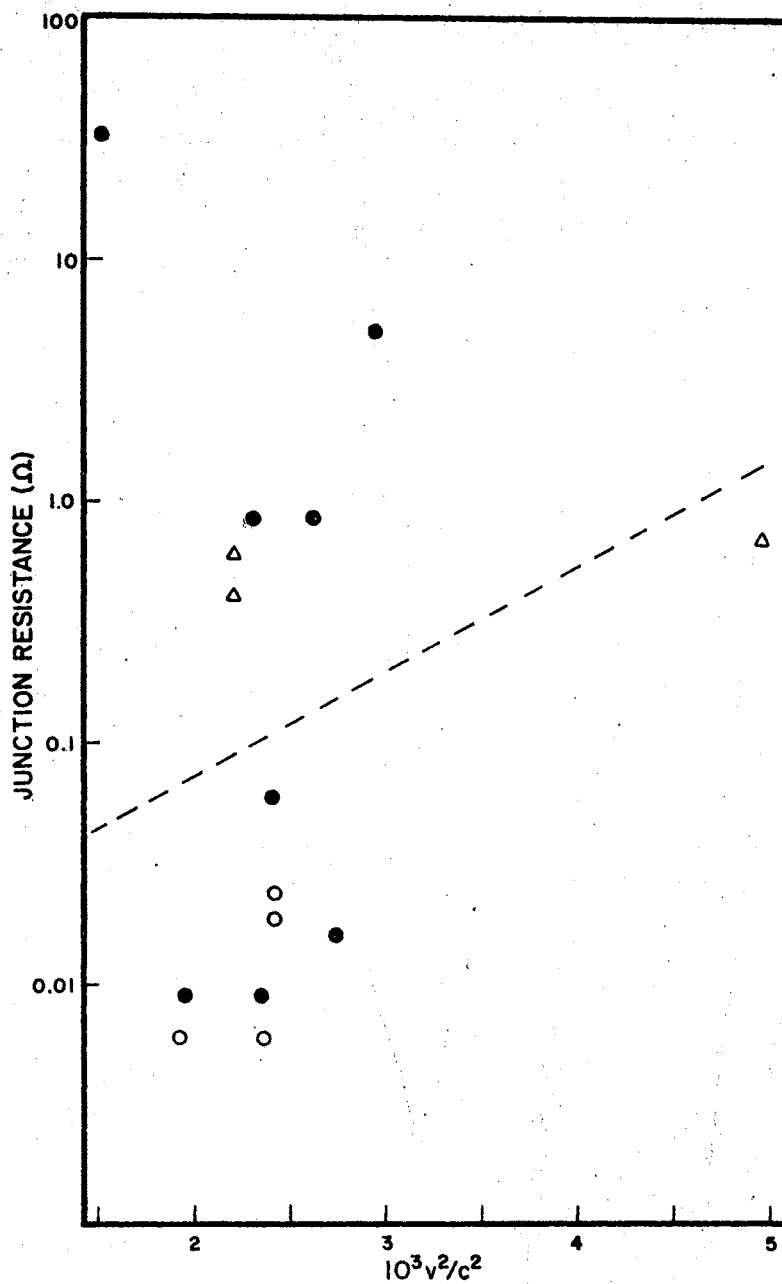


Figure 17. Relationship Between Fiske Mode Velocity and Junction Resistance for a Number of Junctions. Solid figures indicate Pb-I-Pb; open figures, junctions containing Fe; circles, ideal characteristics; triangles, subharmonic structure

and d can be written from the velocity expression by Fiske as

$$d = 2 \left(\frac{v^2}{c^2} \right) \lambda \epsilon,$$

where $d \ll \lambda$, the expected variation with the velocity is

$$\sigma_{NT} \propto \exp \left\{ - \frac{2\lambda\epsilon}{\hbar} [2meV_B]^{1/2} \left(\frac{v^2}{c^2} \right) \right\}.$$

Using Locke's value, $\lambda = 390\text{\AA}$ and order of magnitude numbers, $\epsilon = 10$, and $V_B = 2$ volts, one can estimate the coefficient of v^2/c^2 as 10^3 , which gives the slope of the dotted line in Figure 16. The fact that the observed electromagnetic velocity is virtually independent of junction resistance indicates that the insulator thickness which determines the junction capacitance is different than that which determines the tunneling probability and is also less sensitive to oxidation time. This would be the effect if the oxide is inhomogeneous, with capacitance determined by the average of the reciprocal of the thickness and the tunneling by the average of an exponential function of the thickness.

Subharmonic Structure

A feature which appears in a large number of junctions is always associated with excess currents. The characteristics of two junctions in Figure 18, show excess currents in the I-V characteristics and the subharmonic structure clearly in the derivative. The excess currents below $eV = 2\Delta$ are probably due to small metallic shorts especially in the second junction which shows no extra conductivity at the gap edge. A bridge forms a weak link between the superconductors which couples them more strongly than the tunneling junction. However, the presence

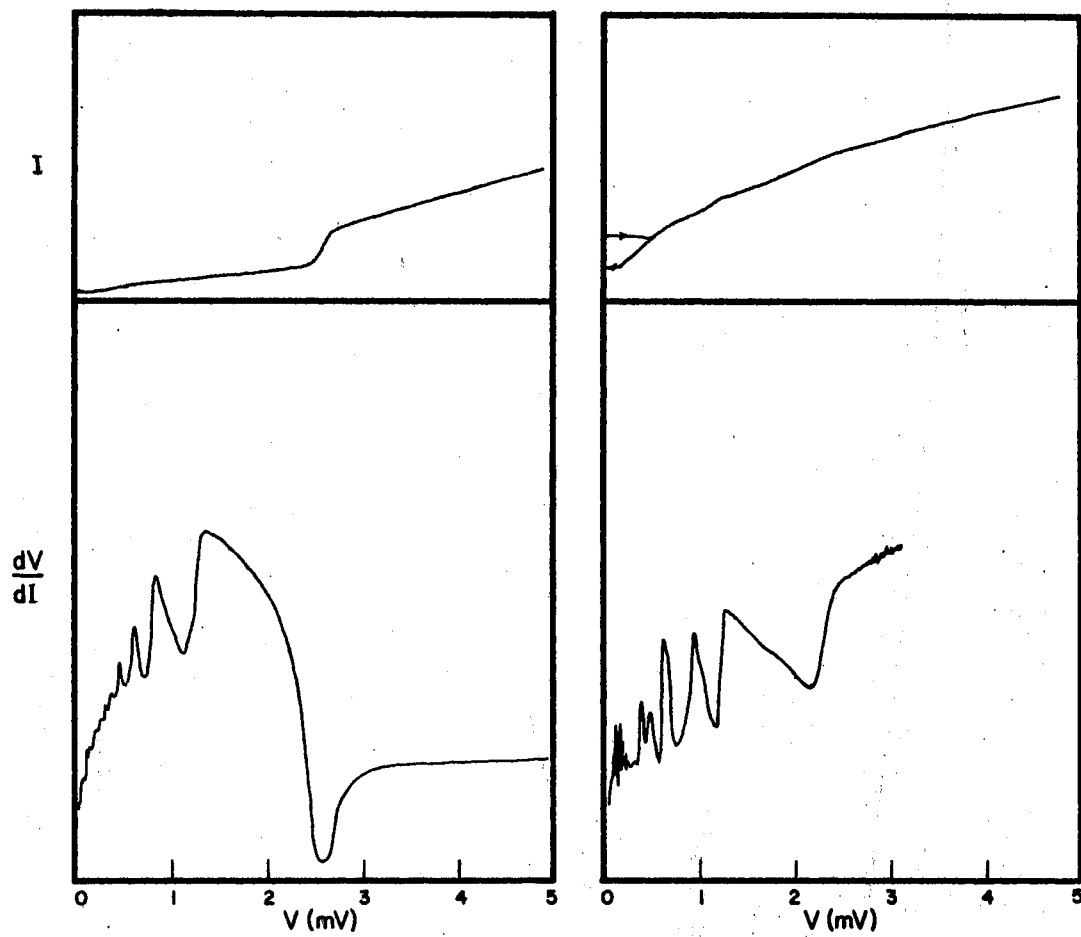


Figure 18. Subharmonic Structure in Two Junctions

of the metallic bridge is not necessary for the appearance of excess currents and subharmonic structure as was demonstrated by Giaever (84) with Cd S barriers which allowed variation of the tunneling probability within the same junction. The fact that a junction shows subharmonic structure, sometimes only detectable in the derivative is thus an indication that there are regions within the barrier thin enough that the matrix element between the states on either side of the junction can no longer be considered small, and the non-linear effects of Josephson tunneling appear. A weak effect at Δ/e as in Figure 11(b), appears in all junctions tested, and may be due to the multiparticle tunneling mechanism proposed by Burstein (85) rather than the self detection mechanism.

CHAPTER IV

FERROMAGNETIC MATERIAL IN TUNNELING JUNCTIONS

The first part of this chapter is devoted to the experiments with the more tractable results. A study is made of the proximity effect between iron and lead as measured by a tunneling probe on the opposite side of the lead. Cooper pairs with energies in the vicinity of the Fermi level are detected for a wide range of lead thicknesses but the current due to these particles is found to decrease exponentially with increasing lead film thickness. This distance dependence is associated with the coherence length of the superconducting lead.

Experiments which are less well understood are discussed in the second part of the chapter. Myriads of interesting effects come from tunneling studies which are unfortunately often ill characterized and sometimes only seen in one sample. A few examples are chosen and some hypotheses proffered.

The junctions used in this investigation have Pb on either side of the barrier with the ferromagnetic film either between the lead films or external to the tunneling junction. These different arrangements allow one to use the tunneling junction as a probe into the behavior of a Pb film whose opposite side is in contact with a ferromagnetic film or vice versa. Of interest also, is whether there are unusual interactions with the tunneling current itself as it passes through a thin ferromagnetic layer. Diagrams of all the arrangements used are in Figure 19.

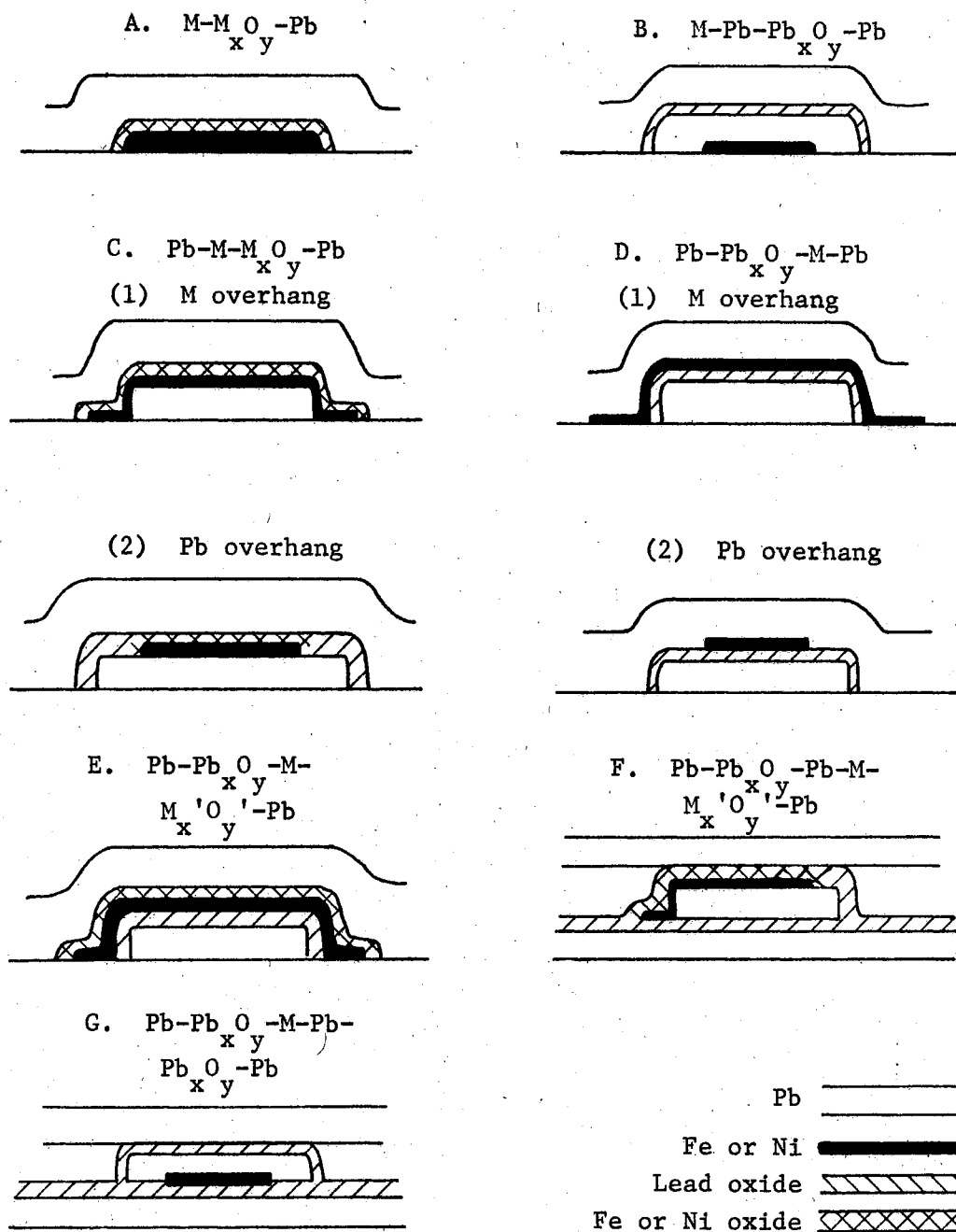


Figure 19. Diagrams of Film Configurations

Since iron and nickel oxidize more slowly than lead, the tunneling probability through the ferromagnetic metal oxide will be much higher ($\sim 10^3$) than through the lead oxide produced simultaneously in configurations C (2) and F. The same result of higher probability of tunneling in the region of the ferromagnetic film is also true for configurations D (2) and G because the evaporation of the ferromagnetic film over lead oxide reduces the tunneling resistance again by orders of magnitude. However, there is less confidence in the current distribution because of lack of knowledge of the nature of the damage to the oxide.

Iron-Lead Tunneling and the Proximity Effect

The simplest arrangement is a tunneling junction with iron and lead forming the conductors and an insulator between. The characteristics of the two samples of this configuration have no startling features and look like normal metal-superconductor tunneling, as can be seen for one sample in Figure 20. The energy gap Δ as measured at the maximum conductance point of the curve is larger than is measured in superconductor-superconductor junctions being 1.50 meV in tunneling from Fe to Pb and 1.55 meV in the opposite direction. This apparent difference in Δ is artifact of superconductor-superconductor tunneling, and the moving of the peak in occupied states over the peak in vacant states as $V \approx 2\Delta/e$. The slightly higher conductance at the band edge for Fe to Pb tunneling is reproduced in all samples also. There are no signs of superconducting states lying within the gap since the steepness of the characteristic at the band edge fits that predicted from the thermal spread about the Fermi level in Fe exactly within the accuracy of the determination ($\approx 2\%$). The phonon structure in Pb is clearly reflected in the characteristic.

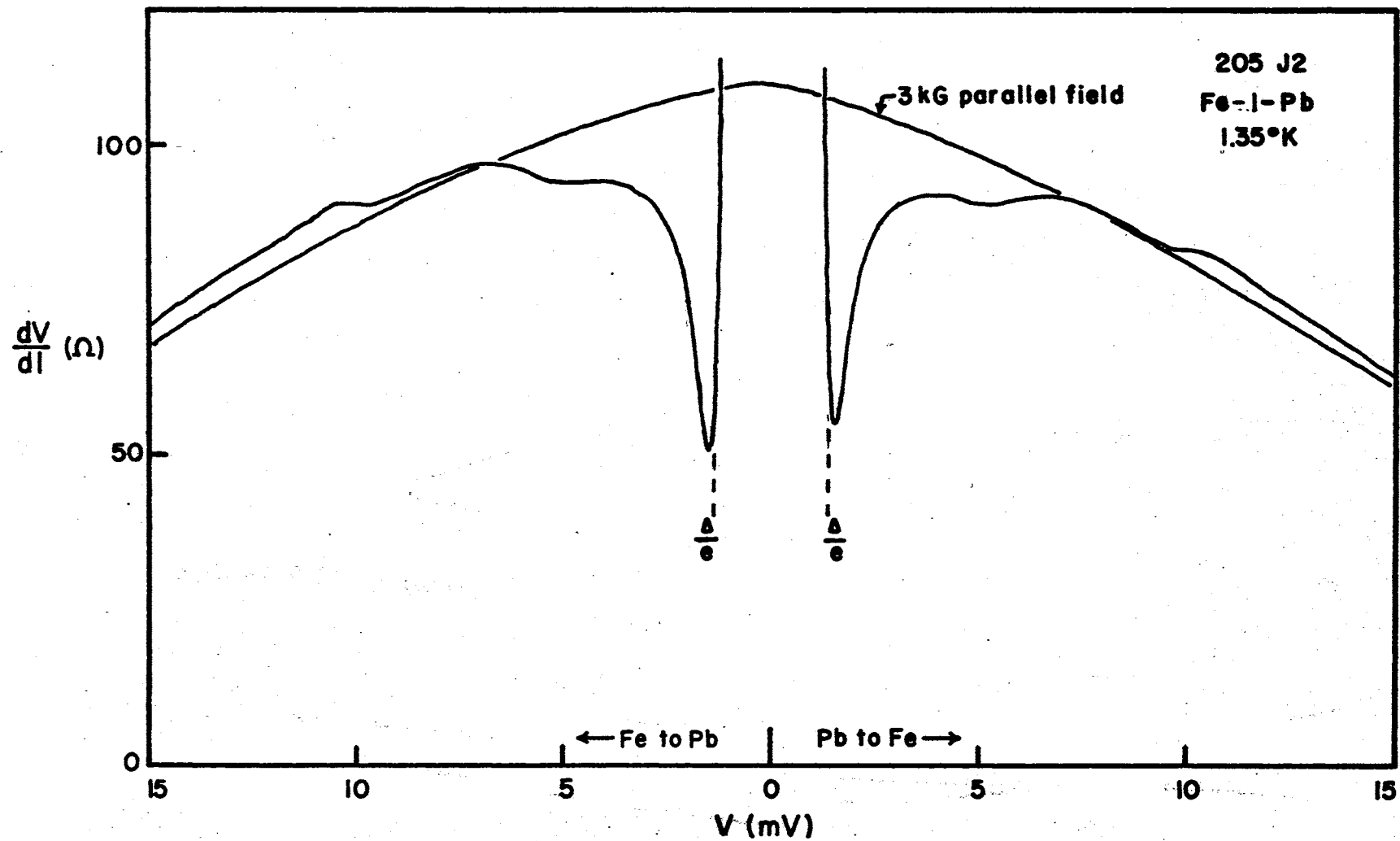


Figure 20. Derivative Characteristics of a Fe-Fe_xO_y Junction

The general decrease in tunneling resistance with increasing emf continues beyond the range plotted in the figure until in the range 20 mV to 90 mV the tunneling current becomes approximately exponential in junction emf. This is a property of the iron oxide barrier and has been observed in tunneling junctions with several metals (154). The magnetic field dependence of the tunneling characteristic shows no sudden transitions caused by switching of the magnetic film and shows the usual smearing of the energy gap as the magnetic field penetrates the superconductor. In summary, the superconductor does not seem to be affected by the presence of the iron film when separated by the iron oxide barrier.

When a ferromagnetic film is deposited adjacent to one of the lead films, a conductivity appears at $eV = \Delta$ increasing to $eV = 2\Delta$ due to a broadening of the superconducting state by the magnetic film. Several M-Pb-I-Pb (configuration B) films were made and the derivative-voltage characteristic in Figure 21 contains some general features:

- (1) The depressed energy gap which is easily compared in this sample to that in the regions of the lead which has no Ni adjacent.
- (2) Increased conductivity over an ordinary lead-lead junction for $eV < 2\Delta$.
- (3) The conductivity around $eV = \Delta$ typical of a normal metal indicating that the energy gap is gone.
- (4) Pair tunneling effects, supercurrents (not shown on derivative plot) and Fiske modes. In these samples it is not clear that the pair effects are not entirely from the regions of the lead not in contact with the magnetic film. Since the size of these regions is about 0.4 mm and the coherence length in lead is only about 900\AA , those regions should act

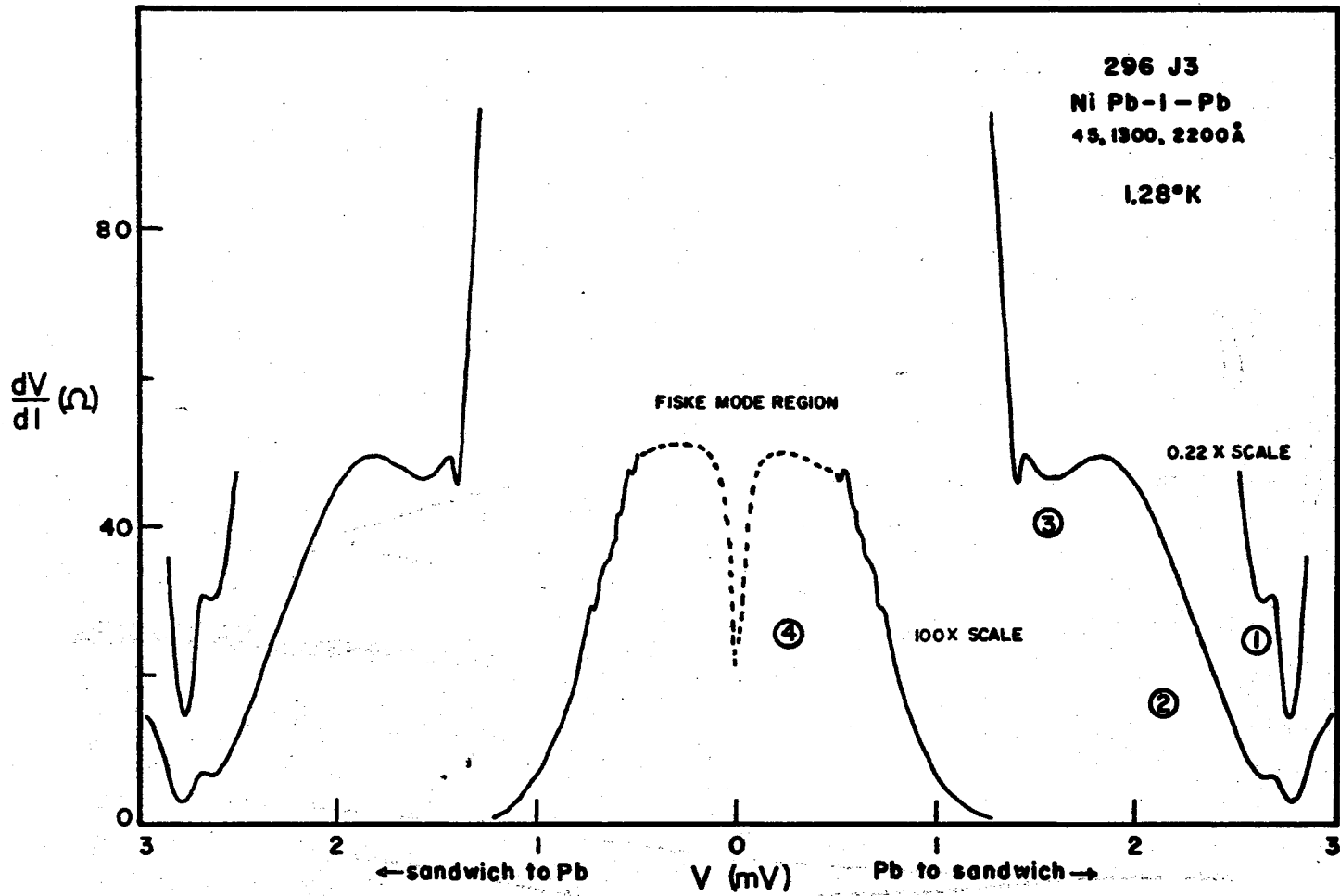


Figure 21. The Effects of Magnetic Films Outside the Junction on Tunneling Characteristics

independently except for magnetic field effects.

Both in the case of magnetic impurities within the bulk of a superconductor and of a magnetic film on the surface, the spread of the edge of the superconducting energy gap is due to a reduction of the pair lifetimes by scattering from the magnetic material (109-111, 113). A difference in the two is that the gapless region in the bulk as predicted by Abrikosov and Gorikov (110) requires a rather critical concentration of magnetic impurity, i.e., greater than 91% of that necessary to destroy superconductivity altogether. However, gaplessness can be induced by proximity with a magnetic film over a wide range of film thickness and superconducting effects can still be observed.

A conductivity ratio R_{σ} is defined to be the ratio of the conductivity in the stationary region just above Δ/e to that in the stationary region just above $2\Delta/e$ and is a measure of the percentage of states at the Fermi level or the "degree of gaplessness". This quantity is plotted for four films as a function of the adjacent Pb film thickness in Figure 22. At large film thicknesses the measured density of states at the center of the gap falls off exponentially with increasing film thickness, as would be expected for a penetration phenomenon. A natural question is whether this extra conductivity due to Cooper pairs whose energy lies near the Fermi level, or to single particles penetrating from a normal region in the immediate vicinity of the Fe. The slope of $\log R_{\sigma}$ vs. Pb thickness gives a characteristic length 935\AA , which is consistent with the breakover near 1000\AA . This change from the exponential relationship is expected when the film is no longer thick with respect to the coherence length and the superconducting state can be characterized by uniform parameters throughout. Thus there is good

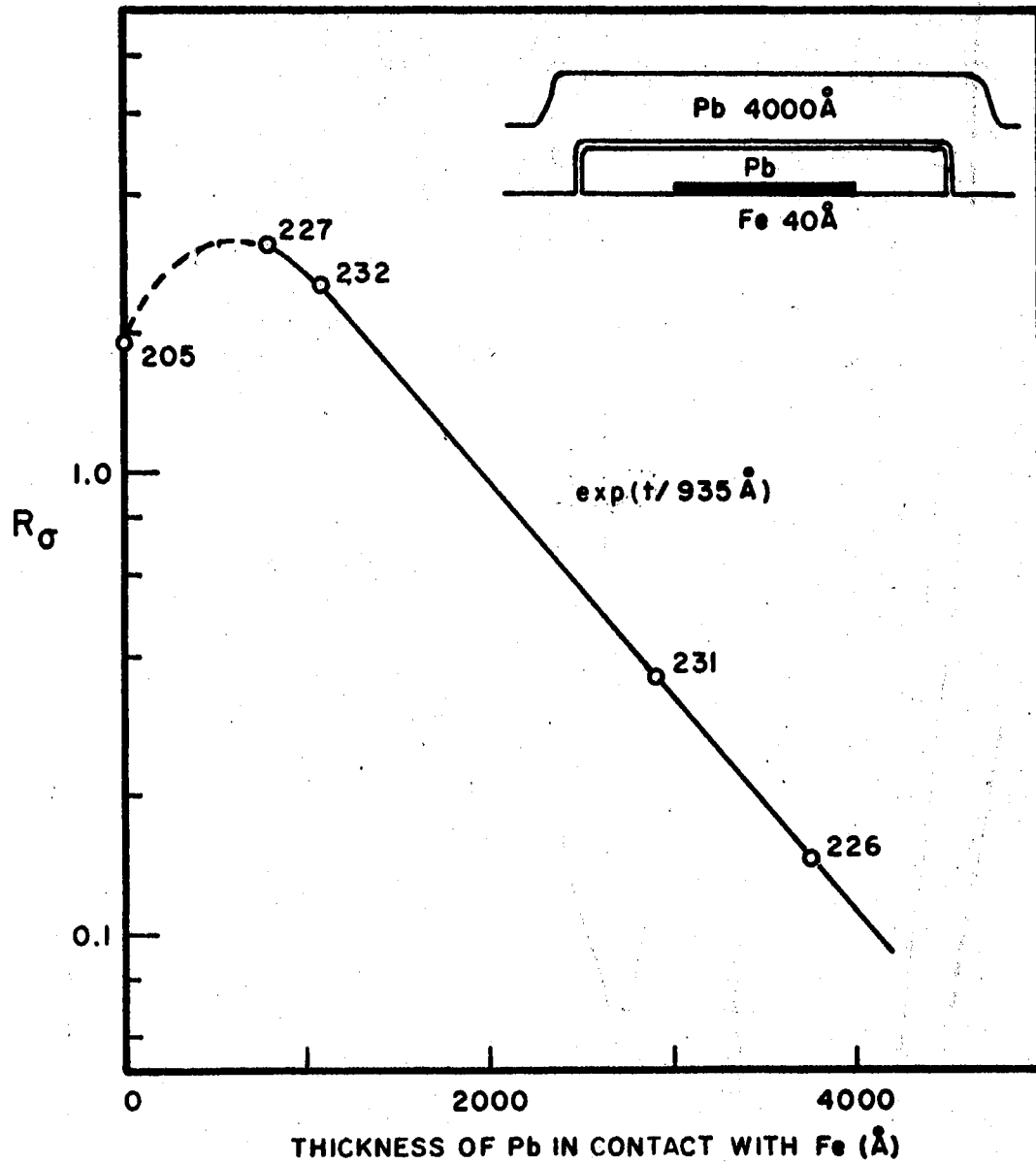


Figure 22. Normalized Density of States Induced at the Fermi Level by the Proximity Effect as a Function of Lead Thickness

reason to associate the 935\AA length with the superconducting coherence length in which case the states near the Fermi level are pair states which cause the extra conductivity. Stronger evidence comes from the slope of the derivative from $2\Delta/e$ down to Δ/e which shows that the density of states decreases monotonically between these points. It is therefore inferred that the conductivity is due to pair states which are spread across the gap, rather than ephermeral electrons whose density would be constant in energy.

Corresponding curves for different materials deposited adjacent to the lead should give the same limiting slope, if the model is correct. If the excess conductivity is due to transient single particles, a junction of the form M-Pb-I-Pb-M showing zero bias conductivity due the proximity effect should not generate strong Fiske modes in the characteristic near zero, in the same sense that thermally excited particles do not. If, however, the proximity effect induces a large number of pairs near the Fermi level, the tunneling characteristic should show electromagnetic resonances in the junction. Thermal spread at the Fermi level might interfere by allowing direct, non-radiative tunneling. The presence of Josephson currents is not a proof of the nature of the particle in question since these currents can arise from the large number of pairs known to be present at the edge of the gap.

Various Effects in Superconducting Junctions

Containing Ferromagnetic Material

When the iron is evaporated so as to be between the lead the tunneling behavior becomes more complicated, partially because of the nature of the tunneling barriers. The evaporation of iron or nickel

films only a few angstroms thick reduces the resistance of lead oxide layers by orders of magnitude and, since there are increases in bridge-like behavior, in a non-uniform manner. The oxidation of the iron or nickel reduces the magnetic film thickness and produces oxides which may be ferromagnetic, antiferromagnetic, or neither. To achieve a minimum coupling between the lead and iron and hopefully to investigate the effect of a ferromagnetic film isolated within a barrier some samples in configuration E were made. The Pb films were approximately 4000\AA thick thus being effectively infinitely thick as far as coherence properties are concerned. The two sample curves in Figure 23 are quite different in that the junction in Figure 23(a) has a voltage dependence of conductance above Δ/e typical of a Pb-I-Pb sample and that in (b) has a conductance comparable to a normal metal-superconductor junction and nearly the same magnitude as above $2\Delta/e$. However, near the energy gap (b) looks very Pb-I-Pb like with no spread of energies, and the edge of the band gap in (a) is broadened distinctly downward about 0.1 mV. There may be ohmic conduction between the Fe film and the Pb layer in (b) to produce the normal metal-superconductor tunneling behavior.

In one of the sample films which has a thermally oxidized 160\AA Fe layer an extra conductance with the appearance of a second energy gap 0.15 mV below the reduced gap appeared the first time the film was tested. As a parallel field was applied the resistance dip broadened and moved downward in voltage at the rate of $2.27 \mu\text{V}/\text{Oersted}$, until it moved into the structure above Δ/e . It did not reappear when the field was reversed or applied normal to the film. The iron was deposited with a stray magnetic field of approximately 90G in the vicinity of the film which should produce an easy axis in the iron film. A possible cause of

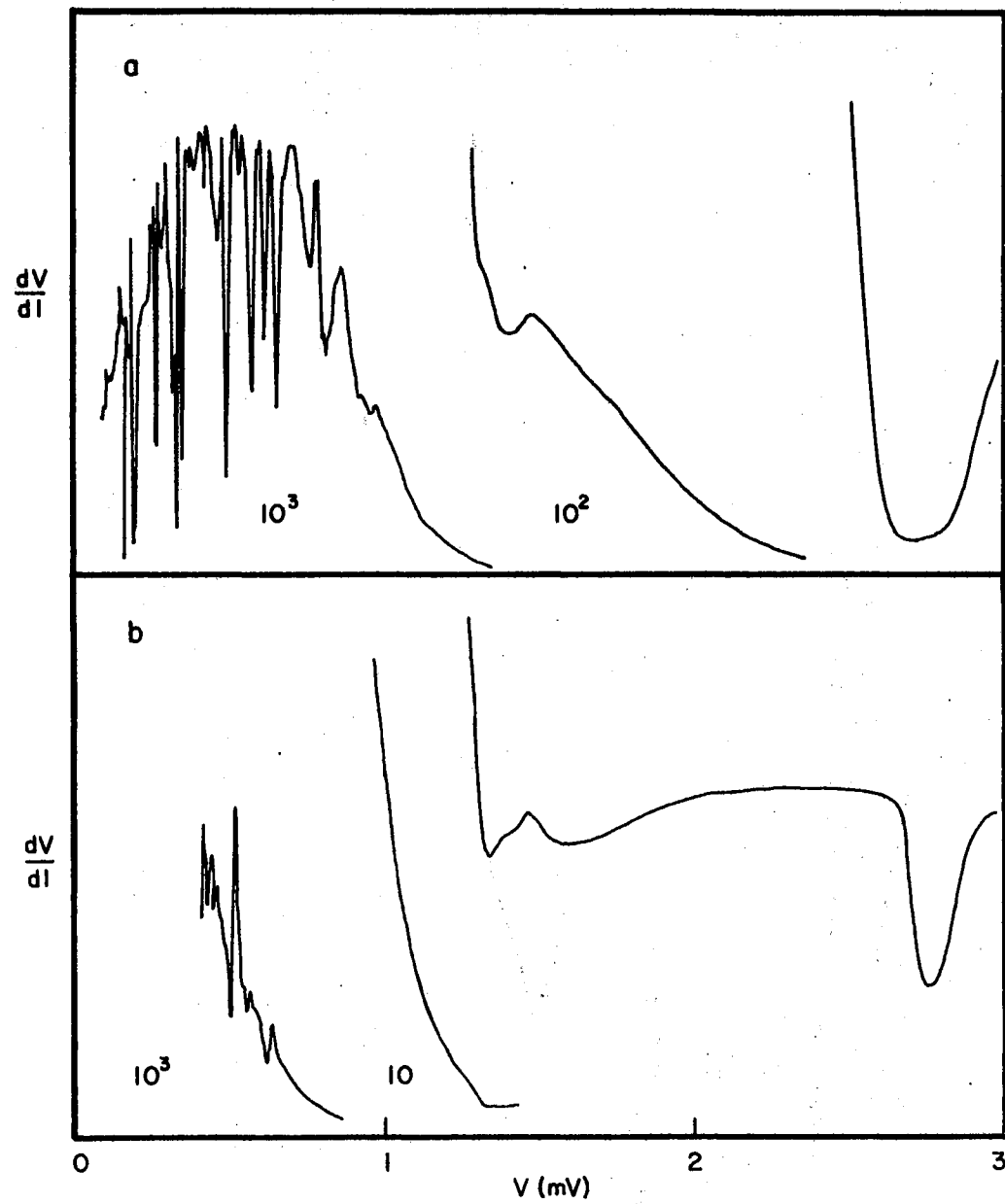


Figure 23. Derivative Curves for Two Pb-I-Fe-I-Pb Samples

the reduced gap is an orientation of domains in the iron film to produce a larger interaction with a region of the Pb film. Flux penetration does not seem to be a likely mechanism since a magnetic field applied to a Pb-I-Pb film primarily produces broadening of the energy gap more than shifts in energy.

Two junctions with an iron film in contact with one of the lead films and an oxide between the iron film and the other lead film have the tunneling structure pictured in Figure 24. The first film has the iron oxidized and the lead deposited on top and the second vice versa. The proximity effect is much reduced and the primary change from a Pb-I-Pb junction is the increased tunneling currents at Δ/e corresponding to $R_G = 0.038$, a much smaller value than would be expected from the results with iron on the side away from the junction. The author believes that the iron film was nearly completely oxidized to reduce the effect so drastically.

The second film shows strong subharmonic structure and supercurrents due to damage to the lead oxide layer during Fe evaporation. Appearance much like this perhaps with the subharmonic structure above Δ/e somewhat suppressed by Fe to Pb tunneling, is typical of junctions made in this configuration.

The junction would have been considered a failure and discarded if it were not for the resistance peaks at 3.35 and 3.89 mV. Application of a magnetic field caused the derivative to bloom with the resistance peaks shown for fields around 2kG in the lower part of the figure. The peak position seems to depend relatively critically upon magnetic field orientation and could not be reproduced if the sample can were moved. The peak voltages are plotted in Figure 25 as a function of parallel

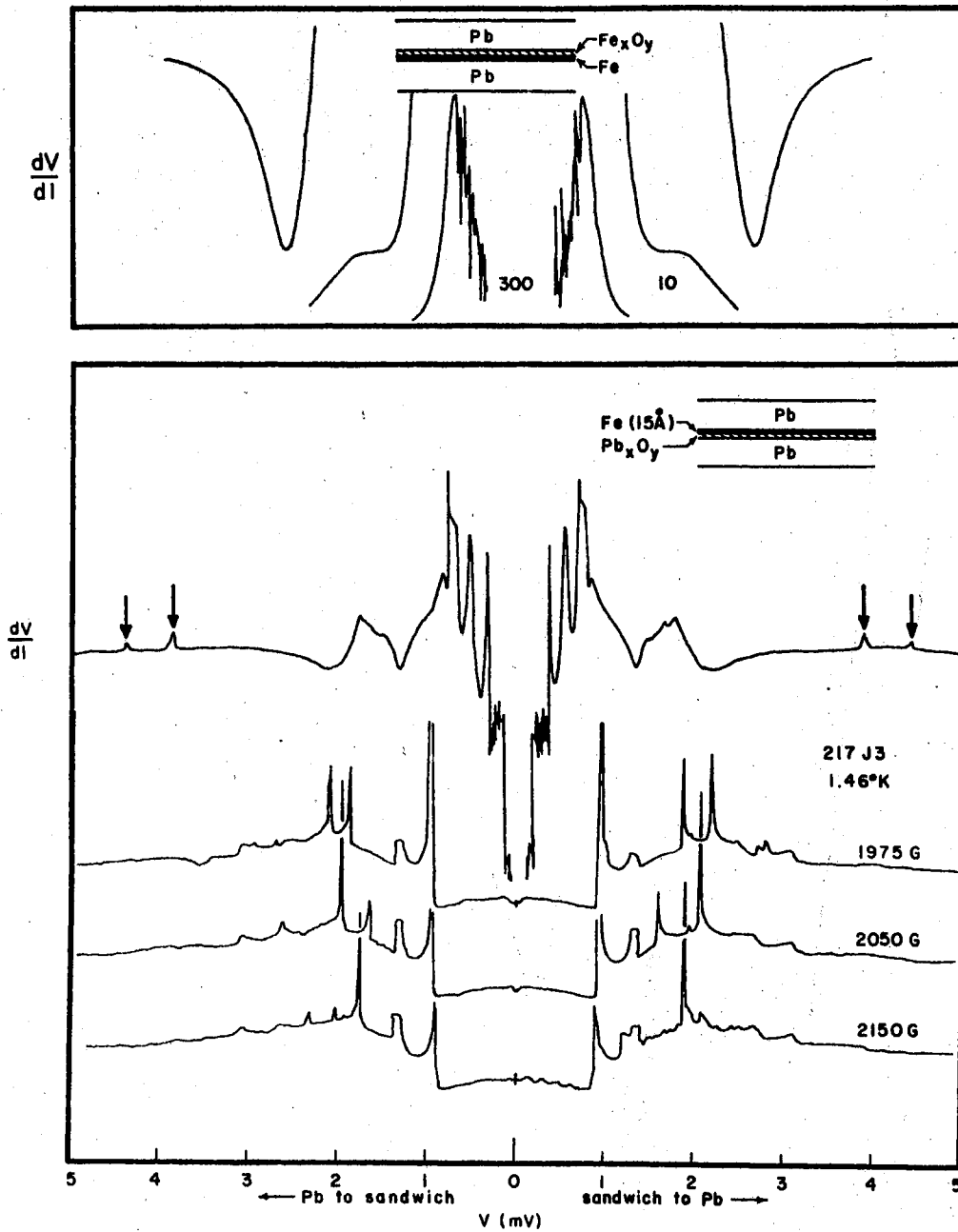


Figure 24. Characteristics of Junctions Containing Fe in Contact With Pb but Within the Barrier

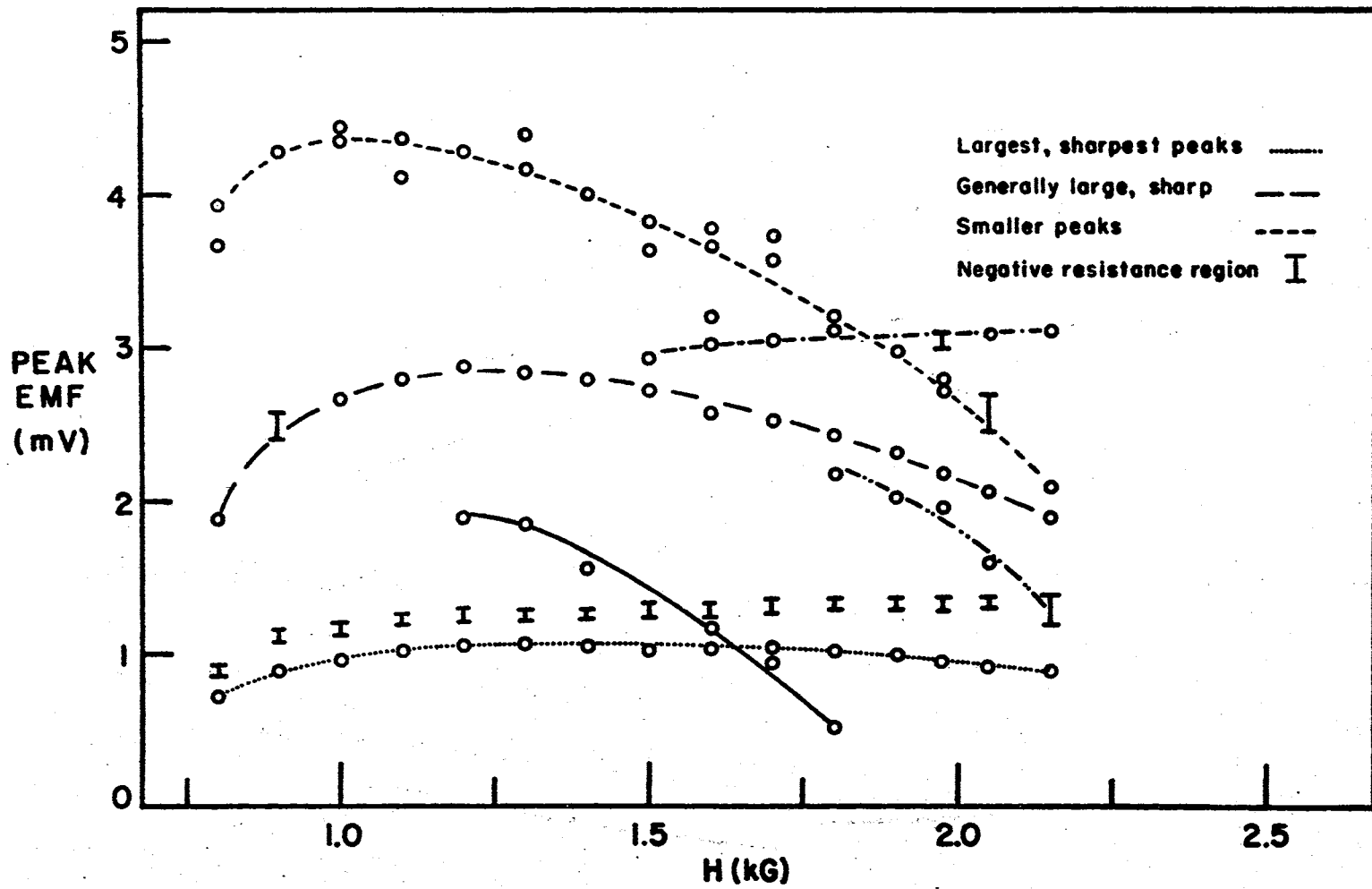


Figure 25. Field Dependence of the Resistance Peaks Shown in Figure 24

magnetic field. The peak position at a field value of 1.99 kG was checked for temperature dependence, the effect of increasing the junction temperature from 1.46 to 2.05 °K is quite similar for nearly all of the peaks to increasing the magnetic field from 1.99 to near 2.13 kG. The temperature dependence and the fact that all moving peaks disappear altogether at a field of 3kG indicate an origin associated with the superconducting state and probably with the bridging. But what is not clear is whether the magnetic film is active in the process or simply produced the bridges originally.

Another type of peak was observed in a much better understood sample, specifically #227J3 which had the thinnest adjacent Pb film in the proximity series (Figure 26). The very sharp high resistance spikes in Figure 24(a) are superimposed on the phonon structure pattern which was much reduced and broadened because of the lack of a sharp band edge. The breadth of the spikes decreased as the field increased until, at the 4.9 and 7.0 kG fields, it became difficult to adjust the bias emf without passing completely through a peak before the derivative system could respond. An attempt was made to track the 13 mV peak at 4.9 kG for small field changes, but with a field change of 50 G the peak disappeared and could not be found even when the field was returned to the former nominal value. The persistence of the spikes for above the critical field makes involvement of the superconducting state less likely. Nonetheless spin wave resonances in the iron film could conceivably couple into the density of superconducting states because of the strong interaction between magnetic phenomena and superconductivity, but a pattern of behavior for the peaks must be established to check any hypotheses.

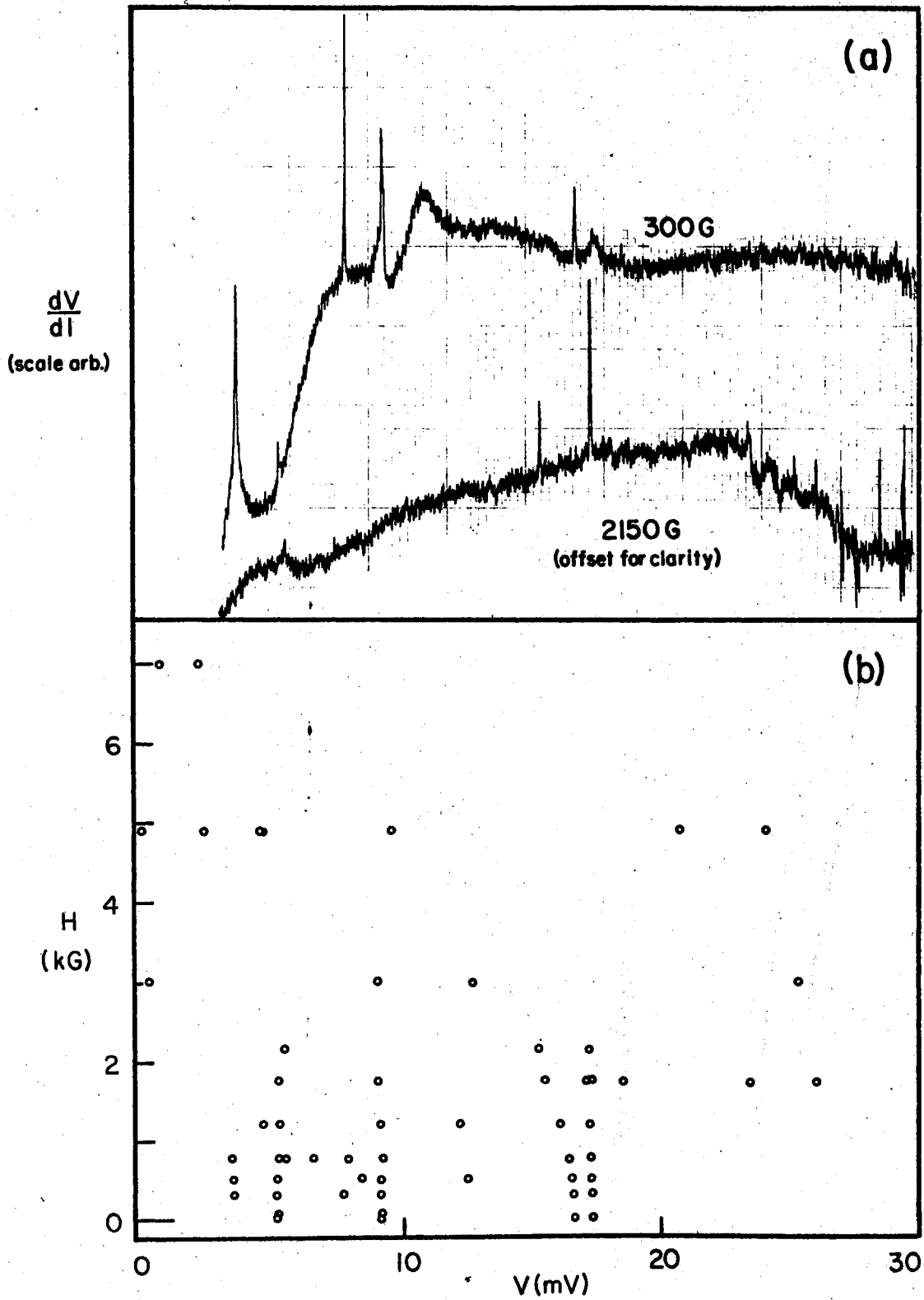


Figure 26. High Resistance Spikes in dV/dI of #227J3 a) Shown Superimposed on the Phonon Structure and b) Magnetic Field at Which Peaks Appear vs. emf of Peak

CHAPTER V

SUMMARY AND SUGGESTED FURTHER WORK

This study has reviewed tunneling in superconducting lead junctions with particular emphasis upon the interaction of ferromagnetic material with the superconducting state. Experimental techniques were described for the fabrication of samples and methods of measurement. A survey of observed phenomena in lead-lead oxide-lead junctions indicated methods of junction characterization which are applicable to other junction types. A study of the proximity effect by the tunneling technique has shown that the superconducting state modified by the adjacent ferromagnetic film penetrates the lead a characteristic distance which is associated with the coherence length of the superconducting state. Some interesting effects which have been observed in junctions containing ferromagnetic material and their possible causes were discussed.

With this background of understanding of superconducting tunneling, the use of the tunneling junction as a detector and possibly a generator of acoustic signals would be a reasonable extension. The coupling between phonons and the superconducting pair is intimate and some of the phenomena discussed in Chapter IV may be linked with phonon or magnon interactions. Initially, the junction would be used as a detector of microwave phonons which would be generated by a quartz transducer and propagated along a sapphire rod to the junction. Detection of phonons by this technique has been observed but the steplike structure similar to

that from photon-irradiation was not observed. A possible technique to improve the sensitivity of the detector would be to make an interferometer of two junctions upon which the phonon will impinge. The separation of the two barriers would be adjusted by choosing the proper film thicknesses to make the stress on one junction out of or in phase with the other. It is well known that an interferometer is very sensitive to changes in magnetic flux, but nothing is known about its sensitivity to acoustic stress.

BIBLIOGRAPHY

- (1) I. Giaever, Phys. Rev. Letters 5, 147, 464 (1960).
- (2) J. E. Mercereau, in Superconductivity, R. D. Parks, Ed. (Marcel Dekker, New York, 1969) pp. 403-420.
- (3) J. W. McWane, J. E. Neighbor and R. S. Newpower, Rev. Sci. Instr. 37, 1602 (1966).
- (4) J. Clarke, Phil. Mag. 13, 115 (1966).
- (5) D. N. Langenberg, W. H. Parker, and B. N. Taylor, Phys. Rev. 150, 186 (1966).
- (6) J. Matisoo, Proc. IEEE 55, 172 (1967).
- (7) H. J. Levinstein, and J. E. Kunzler, Phys. Letters 20, 581 (1966).
- (8) L. J. Barnes, (unpublished).
- (9) J. E. Zimmerman, and A. H. Silver, Phys. Rev. 141, 367 (1966).
- (10) O. M. M. Mitchell and P. P. M. Meincke, IEEE Transactions on Sonics and Ultrasonics SU-15, 66 (1968).
- (11) J. L. Miles and P. H. Smith, J. Electrochem. Soc. 110, 1240 (1962).
- (12) G. J. Tibol and R. W. Hull, J. Electrochem. Soc. 111, 1368 (1964).
- (13) Walter Schroen, J. Appl. Phys. 39, 2671 (1968).
- (14) L. Heijne, J. Phys. Chem. Solids 22, 207 (1961).
- (15) J. R. Anderson and V. B. Tare, J. Phys. Chem. 68, 1482 (1964).
- (16) K. Schwidtal and R. D. Finnegan, Phys. Rev. 2B, 148 (1970).
- (17) L. V. Gregor, IBM Jour. Res. 12, 140 (1968).
- (18) G. Faraci, G. Giaguinta, and N. A. Mancini, Phys. Letters 30A, 400 (1969).
- (19) J. Bardeen, L. N. Cooper, and J. R. Schrieffer, Phys. Rev. 108, 1175 (1957).
- (20) N. V. Zavaritskii, Zh. Eksperm. i Teor. Fiz. 41, 657 (1961).

- (21) I. Giaever and K. Megerle, Phys. Rev. 122, 1101 (1961).
- (22) I. Giaever, H. R. Hart, Jr., and K. Megerle, Phys. Rev. 126, 941 (1962).
- (23) S. Shapiro, P. H. Smith, J. Nicol, J. L. Miles, P. F. Strong, IBM Journ. Res. 6, 34 (1962).
- (24) S. Berman and D. M. Ginsberg, Phys. Rev. 135, 306 (1964).
- (25) R. F. Gasparovic, B. N. Taylor and R. E. Eck, Solid State Comm., 4, 59 (1966).
- (26) P. Kumbhare, P. M. Tedrow and D. M. Lee, Phys. Rev. 180, 519 (1969).
- (27) N. V. Zavaritskii, Zh. Eksperm. i Teor. Fiz. 48, 837 (1965) [Soviet Physics JETP 21, 557 (1965)].
- (28) K. Knorr and N. Barth, Solid State Comm. 6, 791 (1968).
- (29) Y. Goldstein, Rev. Mod. Phys., 36, 213 (1964).
- (30) P. W. Anderson, Proc. of the Seventh Intern. Conf. on Low Temp. Phys., G. M. Graham and A. C. Hollis Hallet, Eds. (Univ. Toronto Press, Toronto, 1961) p. 304.
- (31) G. M. Eliashberg, Zh. Eksperm. i. Teor. Fiz. 38, 966 (1960) [Soviet Phys. JETP 11, 696 (1960)].
- (32) J. M. Rowell, P. W. Anderson, and D. E. Thomas, Phys. Rev. Letters 10, 334 (1963).
- (33) J. M. Rowell, Rev. Mod. Phys. 36, 199 (1964).
- (34) P. Morel and P. W. Anderson, Phys. Rev. 125, 1263 (1962).
- (35) J. R. Schrieffer, D. J. Scalapino, and J. W. Wilkins, Phys. Rev. Letters 10, 336 (1963).
- (36) J. R. Schrieffer, Rev. Mod. Phys. 36, 200 (1964).
- (37) D. J. Scalapino, Rev. Mod. Phys. 36, 205 (1964).
- (38) D. J. Scalapino and P. W. Anderson, Phys. Rev. 133, A 921 (1964).
- (39) D. J. Scalapino, Y. Wada, and J. C. Swihart, Phys. Rev. Letters 14, 102 (1965).
- (40) J. C. Swihart, D. J. Scalapino, Y. Wada, Phys. Rev. Letters 14, 106 (1965).
- (41) W. L. McMillan and J. M. Rowell, Phys. Rev. Letters 14, 108 (1965).

- (42) B. M. Brockhouse, T. Arose, G. Caglioti, K. R. Rao and A. D. B. Woods, Phys. Rev. 128, 1099 (1962).
- (43) R. C. Dynes, J. P. Carbotte, and E. J. Woll, Jr., Solid State Comm. 6, 101 (1968).
- (44) J. P. Carbotta and R. C. Dynes, Phys. Rev. 172, 476 (1968).
- (45) J. M. Rowell, W. L. McMillan and W. L. Feldman, Phys. Rev. 178, 897 (1969).
- (46) R. Stedman, L. Almqvist, G. Nilsson and G. Raunio, Phys. Rev. 162, 545 (1967); 163, 567 (1967); R. Stedman, L. Almqvist, and G. Nilsson, *ibid.* 162, 549 (1967).
- (47) J. M. Rowell and L. Kopf, Phys. Rev. 137, 907 (1965).
- (48) J. G. Adler, J. S. Rogers, and S. B. Woods, Can. J. Phys. 43, 557 (1965).
- (49) L. Y. L. Shen, Phys. Rev. Letters 24, 1104 (1970).
- (50) Iu. V. Medvedev, Izvestia V. U. Z., Fizika, 11; 137 (1968).
- (51) P. W. Wyatt and A. Yelson, Phys. Rev. 2B, 4461 (1970).
- (52) B. D. Josephson, Phys. Letters 1, 251 (1962).
- (53) P. W. Anderson and J. M. Rowell, Phys. Rev. Letters 10, 230 (1963).
- (54) J. M. Rowell, Phys. Rev. Letters 11, 200 (1963).
- (55) P. W. Anderson in Lectures on the Many Body Problem, E. R. Caianello, Ed. (Academic Press, New York, 1964), Vol. 2, p. 113.
- (56) B. D. Josephson, Rev. Mod. Phys. 36, 216 (1964).
- (57) I. K. Yanson, V. M. Svistunov and I. M. Dmitrenko, Soviet Phys. JETP 20, 1404 (1965).
- (58) J. E. Nordman, J. Appl. Phys. 40, 2111 (1969).
- (59) R. A. Ferrell and R. E. Prange, Phys. Rev. Letters 10, 479 (1963).
- (60) Walter Schroen and J. Paul Pritchard, Jr., J. Appl. Phys. 40, 2118 (1969).
- (61) K. Schwidtal and R. D. Finnegan, J. Appl. Phys. 40, 2123 (1969).
- (62) V. Ambegaokar and A. Baratoff, Phys. Rev. Letters 10, 486 (1963).
- (63) T. A. Fulton and D. E. McCumber, Phys. Rev. 175, 585 (1968).
- (64) B. D. Josephson, Advan. Phys. 14, 419 (1965).

- (65) Yu. M. Ivanchenko, Zh. Eksper. i. Teor. Fiz., Pisma v. Redaktsiu 8, 189 (1968) [Soviet Physics JETP 8, (1968)].
- (66) J. T. Anderson and A. M. Goldman, Phys. Rev. Letters 23, 128 (1969).
- (67) I. O. Kulik, Zh. Eksperim. i Teor. Fiz. 49, 1211 (1965 [Soviet Phys. JETP 22, 841 (1966)]).
- (68) R. C. Dynes and T. A. Fulton, Phys. Rev. B 3, 3015 (1971).
- (69) S. Shapiro, Phys. Rev. Letters 11, 80 (1963).
- (70) A. H. Dayem and R. J. Martin, Phys. Rev. Letters 8, 246 (1962).
- (71) P. K. Tien and J. P. Gordon, Phys. Rev. 129, 647 (1963).
- (72) N. K. Werthamer, Phys. Rev. 147, 255 (1966).
- (73) G. E. Everett in Tunneling Phenomena in Solids, E. Burstein and S. Lundqvist, Ed. (Plenum Press, New York, 1969), Chp. 25, p. 353.
- (74) D. N. Langenberg, *ibid.*, Chp. 33, p. 519.
- (75) C. K. Bak, N. Zeuthen Heidam, B. Kofoed, N. Falsig Pedersen, K. Saermark, O. H. Sorensen, S. Teller, 4th Nordic Solid State Conference (abstracts), Turku, Finland 1970. (Univ. Turku, Turku, Finland, 1970) p. 36.
- (76) C. A. Hamilton and Sidney Shapiro, Phys. Rev. 2B, 4494 (1970).
- (77) W. H. Parker, D. N. Langenberg, A. Denenstein and B. N. Taylor, Phys. Rev. 177, 639 (1969).
- (78) M. D. Fiske, Rev. Mod. Phys. 36, 221 (1964).
- (79) D. D. Coon and M. D. Fiske, Phys. Rev. 138, A471 (1965).
- (80) I. K. Yanson, V. M. Svistunov and I. M. Dmitrenko, Zh. Eksperim i. Teor Fiz. 48, 976 (1965) [Soviet Phys. JETP 21, 650 (1965)].
- (81) Michael J. Stephen, Phys. Rev. 182, 531 (1969).
- (82) A. J. Dahm, A. Denenstein, D. N. Langenberg, W. H. Parker, D. Rogovin and D. J. Scalapino, Phys. Rev. Letters 22, 1416 (1969).
- (83) R. A. Kamper and J. E. Zimmerman, J. Appl. Phys. 42, 132 (1971).
- (84) I. Giaever and H. R. Zeller, GE Res. and Dev. Center Report No. 69-C-371 (1969).
- (85) B. N. Taylor and E. Burstein, Phys. Rev. Letters 10, 14 (1963).

- (86) J. R. Schrieffer and J. W. Wilkins, Phys. Rev. Letters 10, 13 (1963).
- (87) C. J. Adkins, Phil. Mag. 8, 1051 (1963).
- (88) C. J. Adkins, Rev. Mod. Phys. 36, 211 (1964).
- (89) I. K. Yanson, V. H. Svistunov and I. M. Dmitrenko, Soviet Phys. JETP, 20, 1404 (1965); 23, 650 (1965).
- (90) I. K. Yanson and I. kh Albegova. Soviet Phys. JETP 28, 826 (1969).
- (91) J. M. Rowell and W. L. Feldman, Phys. Rev. 172, 393 (1968).
- (92) S. Shapiro, J. Appl. Phys. 38, 1879 (1967).
- (93) W. J. Tomasch, Phys. Rev. Letters 15, 672 (1965).
- (94) J. M. Rowell and W. L. McMillan, Phys. Rev. Letters 16, 453 (1966).
- (95) W. L. McMillan and P. W. Anderson, Phys. Rev. Letters 16, 85 (1966).
- (96) R. C. Jaklevic, John Lambe, M. Mikkor, and W. C. Vassel, Phys. Rev. Letters 26, 88 (1971).
- (97) J. Lambe and R. C. Jaklevic, Phys. Rev. 165, 821 (1968).
- (98) R. C. Jaklevic and J. Lambe in Tunneling Phenomena in Solids, E. Burstein and S. Lundqvist, Ed. (Plenum Press, New York, 1969) Chp. 17-18.
- (99) R. C. Jaklevic and J. Lambe, Phys. Rev. B 2, 808 (1970).
- (100) Hollis L. Caswell, J. Appl. Phys. 32, 105 (1963).
- (101) J. C. Fisher and I. Giaever, J. Appl. Phys. 32, 172 (1961).
- (102) A. F. G. Wyatt, Phys. Rev. Letters 13, 401 (1964).
- (103) J. M. Rowell and L. Y. L. Shen, Phys. Rev. Letters 17, 15 (1966).
- (104) P. W. Anderson, Phys. Rev. Letters 17, 95 (1966).
- (105) J. Appelbaum, Phys. Rev. Letters 17, 91 (1966); Phys. Rev. 154, 633 (1967).
- (106) A. F. G. Wyatt and D. J. Lythall, Phys. Rev. Letters 25A, 541 (1967).
- (107) J. E. Christopher, R. V. Coleman, Acar Isin, and R. C. Morris, Phys. Rev. 172, 485 (1968).

- (108) H. R. Zeller and I. Giaever, Phys. Rev. 181, 789 (1969).
- (109) B. T. Matthias, H. Suhl, and E. Correnzwit, Phys. Rev. Letters 1, 92 (1958); J. Phys. Chem. Solids 13, 156 (1969).
- (110) A. A. Abrikosov and L. P. Gorikov, Soviet Phys. JETP 12, 1243 (1961).
- (111) P. Fulde, H. F. Hoenig, Solid State Comm. 8, 341 (1970).
- (112) M. A. Wolf and F. Reif, Phys. Rev. 137, A557 (1965).
- (113) W. L. McMillan, Phys. Rev. 175, 537 (1968).
- (114) A. B. Kaiser and M. J. Zuckerman, Phys. Rev. B1, 229 (1970).
- (115) P. H. Smith, S. Shapiro, J. L. Miles and J. Nicol, Phys. Rev. Letters 6, 686 (1961).
- (116) H. Meissner, Phys. Rev. 117, 672 (1960); IBM J. Res. Dev. 6, 71 (1962).
- (117) E. J. Adkins and B. W. Kington, Phys. Rev. 177, 777 (1969).
- (118) S. M. Freake and C. J. Adkins, Phys. Letters 29A, 382 (1969).
- (119) D. H. Prothero, S. M. Freake and C. J. Adkins (unpublished).
- (120) P. G. de Gennes and E. Guyon, Phys. Letters 3, 168 (1963).
- (121) J. J. Hauser, H. C. Theurer and N. R. Werthamer, Phys. Rev. 136, A637 (1964).
- (122) G. Deutscher and P. G. de Gennes in Superconductivity, R. D. Parks, Ed. (Marcel Dekker, New York, 1969) Vol II, pp. 1005-1033.
- (123) P. Hilsch and R. Hilsch, Z. Physik 180, 10 (1964).
- (124) J. J. Hauser, H. C. Theurer, and N. R. Werthamer, Phys. Rev. 142, 118 (1966).
- (125) F. Meunier, J. P. Burger, G. Deutscher and P. A. Van Dalen, Phys. Letters 24A, 722 (1967).
- (126) J. J. Hauser, Phys. Rev. Lett. 23, 374 (1969).
- (127) A. C. Rose-Innes and B. Serim, Phys. Rev. Letters 7, 278 (1961).
- (128) J. J. Hauser, Phys. Rev. 164, 558 (1967).
- (129) J. J. Hauser, Phys. Rev. 187, 580 (1969).

- (130) P. Fulde and K. Maki, *Phys. Condensed Matter* 5, 380 (1966).
- (131) L. Kleinman, B. N. Taylor and E. Burstein, *Rev. Mod. Phys.* 36, 208 (1969).
- (132) E. Lax and F. L. Vernon, Jr., *Bull. Am. Phys. Soc.* 9, 713 (1964).
- (133) E. Lax and F. L. Vernon, Jr., *Phys. Rev. Letters* 14, 256 (1965).
- (134) Y. Goldstein and B. Abeles, *Phys. Letters* 14, 78 (1965).
- (135) Y. Goldstein, B. Abeles, and R. W. Cohen, *Phys. Rev.* 151, 349 (1966).
- (136) R. W. Cohen, *Phys. Letters A* 33a, 271 (1970).
- (137) W. Eisenmenger and A. H. Dayhem, *Phys. Rev. Letters* 18, 125 (1967).
- (138) W. Eisenmenger in Tunneling Phenomena in Solids, E. Burstein and S. Lunqvist (Plenum Press, New York, 1969) pp. 371-384.
- (139) J. P. Schulz, O. Weis, *Phys. Letters A* 32a, 381 (1970).
- (140) Tewordt, L., *Phys. Rev.* 127, 371 (1962); 128, 12 (1962).
- (141) L. Hollard, Vacuum Deposition of Thin Films (John Wiley and Sons, New York, 1956) Chp. 14.
- (142) E. H. Holt and R. E. Haskell, Foundations of Plasma Dynamics (Macmillan, New York, 1965) Chp. 15.
- (143) W. H. Keesom and A. P. Keesom, *Physica* 3, 359 (1936).
- (144) J. F. Allen, R. Peierls and M. Zaki Uddin, *Nature* 140, 62 (1937).
- (145) B. B. Goodman, *Proc. Phys. Soc. (London)* A66, 217 (1953).
- (146) W. S. Corak, B. B. Goodman, C. B. Satterthwaite, and A. Wexler, *Phys. Rev.* 102, 656 (1956).
- (147) W. Meissner and R. Ochsenfeld, *Naturwiss.* 21, 787 (1933).
- (148) F. London and H. London, *Proc. Roy. Soc. (London)* A149, 71 (1935).
- (149) F. London and H. London, *Physica* 2, 341 (1935).
- (150) J. M. Locke, *Proc. Roy. Soc. (London)* A208, 391 (1951).
- (151) V. L. Ginzburg and L. D. Landau, *Ah. Eksperim. i. Teor. Fiz.* 20, 1064 (1950).
- (152) C. S. Owen and D. J. Scalapino, *Phys. Rev.* 164, 538 (1967).

- (153) A. M. Goldman and P. J. Kreisman, Phys. Rev. 164, 544 (1967).
- (154) R. C. Morris, J. E. Christopher and R. V. Coleman, Phys. Rev. 184, 565 (1969).

VITA

Joe Francis Guess

Candidate for the Degree of

Doctor of Philosophy

Thesis: EFFECTS OF FERROMAGNETIC LAYERS UPON TUNNELING IN SUPERCONDUCTING LEAD JUNCTIONS

Major Field: Physics

Biographical:

Personal Data: Born in Chickasha, Oklahoma, January 9, 1940, the son of Joe D. and Mary L. Guess.

Education: Graduated from Bethany High School, Bethany, Oklahoma, in May, 1957; received the Bachelor of Science degree in Physical Science from Bethany Nazarene College in May 1960; received the Master of Science degree from Oklahoma State University in May 1963; enrolled in doctoral program at Oklahoma State University, 1963-1965; completed requirements for the Doctor of Philosophy degree at Oklahoma State University in May, 1972.

Professional Experience: Graduate Teaching Assistant, Physics Department, Oklahoma State University, 1960-1961; graduate research assistant, Physics Department, Oklahoma State University, 1961-1965; Instructor: Eastern Nazarene College, 1965-1966; Research Engineer: Sylvania Applied Research Laboratory, 1966-1968; graduate teaching assistant, Physics Department, Oklahoma State University, 1968-1969; graduate research assistant, Physics Department, Oklahoma State University, 1969-1971.